

**EXPERIMENTAL AND NUMERICAL INVESTIGATION OF THE INFLUENCE
OF CABLES ON UTILITY POLE MODAL PROPERTY EXTRACTION**

By

©Plínio Ferreira Pinto

A Thesis Submitted to the

School of Graduate Studies

in Partial Fulfilment of the Requirements for the Degree of

Master of Engineering

Faculty of Engineering and Applied Science

Memorial University of Newfoundland

May, 2017

St. John's

Newfoundland and Labrador

Canada

Abstract

This work is a preliminary study on the dynamic response of poles with and without the influence of electrical lines. It is part of a research collaboration between NL Hydro and Memorial University of Newfoundland to achieve a better method of diagnosing aging wooden poles through non-destructive techniques. Previous researchers in this collaboration have found a good correlation between modal testing and wooden pole decay when the poles were tested in the laboratory. However, this correlation weakens with results from field tests, possible due to foundation or attached cables. Therefore, the main objectives of this research are to create a dynamic model for a pole and cable, to design an experimental rig of a reduced scale pole and cable, to use the experimental rig to validate those models, and to gain insights on the influences of the cable on the pole response for future research. The pole model consists of a Euler-Bernoulli cantilever beam obtained through the separation of variables method. The cable was modeled by using a lumped segmentation technique that considers the system as a sum of several lumped elements containing mass, ideal springs and viscous dampers. Both models are implemented using the commercial software *20sim*, which is a graphical solver for the bond graph formalism that simplifies the process of building, assembling and testing the models. These models are intended to be preliminary tools for future work with trustable simulations, thus will allow for the study of the interaction between systems, the scaling of long transmission lines and their effects on the results of modal testing, and the insertion of other electric components and attachments usually found holding the cables on the poles (i.e. isolators, cross arms, ground wire, guy wires, etc.). A reduced physical model for the pole and cable

is designed to proceed with the validation of the developed models. Modal testing and time series measurements are performed over the apparatus and compared with the simulation results, showing good comparative results. In addition, the methods developed, physical and computational, can be used in the continuation of this work.

Acknowledgements

I want to acknowledge and thank the many people that directly or indirectly were involved in this study.

I feel that I'm blessed for being concluding this work and I thank God for everything.

I want to express my gratitude especially to Dr. Geoff Rideout for the opportunity, patience, and supervision, not only providing information but also guidance and suggestions from the beginning to the end of this work. Your enthusiasm, hard work and dedication are inspiring!

I am also grateful to Newfoundland Hydro, Dr. Asim Haldar and Mr. Andre Marshall for the funding, provided materials and technical support.

In addition, I want to acknowledge and thank the staff members of the Faculty of Engineering and Applied Science of Memorial University of Newfoundland, especially Matthew Curtis, Tom Pike, Trevor Clark, David Snook and Jerry Smith.

I am also grateful to all my dear friends, this multicultural team, that have always provided great support through these years, especially Aninda Mondal, Rioko Mine-Goldring, Regina A. Hurley, Mohammad Parsazadeh, Peng Yu, Vahit Saydam, Silvana Pereira, Naveel Islam, and Suvra Chakraborty.

In conclusion, I want to express my gratitude for the constant motivation, love and support of my mother Suzi H. S. Pinto, father Claudine F. Pinto and brothers, José and Miguel.

Even when you are distant you are always with me!

Thank you.

Table of Contents

Abstract	i
Acknowledgements	iii
List of Tables	vii
List of Figures	viii
List of Symbols and Abbreviations.....	x
List of Appendices	xiii
Chapter 1 - Introduction.....	1
Research Proposal.....	2
Chapter 2 - Literature Review.....	5
Non-destructive Methods.....	5
Background for Cable Modeling Theory, Experiments and Simulation	9
Chapter 3 - Research Methods.....	14
Bond Graphs	14
Modal Testing.....	17
Performing a Modal Test	18
Chapter 4 - Pole Modeling	23
Modeling an Euler-Bernoulli Beam through Distributed Parameters.....	23
Bond Graph Implementation of an Euler-Beam (Modal Expansion)	26
Proposing a Physical Model for Testing the Pole Model	30

Modifications for Adding Damping.....	31
Chapter 5 - Cable Modeling.....	32
Lumped-Segmentation Model	32
Modeling a Cable through Lumped Segmentation	33
Bond Graph Implementation of a Cable	36
Cable Bond Graph on the Connection Points	38
String Equation	39
Proposing a Physical Model for Testing the Cable Model	40
Adding the Third Dimension	41
Chapter 6 - Proposed Tests for Model Verification.....	44
Pole and Cable Materials	44
Modal Testing Procedures	45
Time Series Procedures.....	46
Procedures for Adding Damping to the Bar.....	48
Chapter 7 - Model Verification and Added Damping: Results and Discussion	49
Verifying the Pole Model.....	49
Verifying the Cable Model	51
Cable and Pole Model Verification.....	54
Additional Damping and System Behaviour	57

Chapter 8 - Conclusions and Future Work.....	61
Future Work	62
Bibliography	65

List of Tables

Table 3.1. Equipment for Modal Testing and Tension Measurements	20
Table 6.1. Materials Properties	44
Table 7.1. Pole Frequency Response, Modal Testing and Simulation (Pinto & Rideout, 2016)	50
Table 7.2. Cable Frequencies: Theoretical, Modal Test and Simulation. (Pinto & Rideout, 2016)	52
Table 7.3. Sagged Cable Measurements	52
Table 7.4. Bar-Cable System Frequency Response, Modal Testing and Simulation (Pinto & Rideout, 2016)	54
Table 7.5. Results of Modal Testing on Bar and Cable with/without Additional Damping.	59

List of Figures

Figure 1.1. Schematics of Pole - Cable System (Pinto & Rideout, 2016)	3
Figure 3.1. Bond Graph of a Generic System and its Elements (Extracted from Karnopp, et al. (2012)).....	15
Figure 3.2. Mechanical and Electrical Systems in Bond Graph Representation	16
Figure 3.3. Schematics of a Generic Modal Test of a Beam Using Hammer Excitation .	19
Figure 3.4. Generic Stabilization Chart Analysis Generated with ModalVIEW	22
Figure 4.1. Cantilever Euler-Bernoulli Beam Considering Five Modes (Pinto & Rideout, 2016)	29
Figure 5.1. Element of Spring (K), Damper (B) and Mass (M) of a Cable (Pinto & Rideout, 2016)	34
Figure 5.2. Equilibrium of Forces on Two Elements of the Cable on the X-Y Plane (Pinto & Rideout, 2016)	34
Figure 5.3. Element of Spring/Damper and Mass in Bond Graph (Pinto & Rideout, 2016)	37
Figure 5.4. Termination Element of Cable (Pinto & Rideout, 2016).....	38
Figure 5.5. Connector with and without Load Cell and Threaded Rod to Hold the Cable	40
Figure 5.6. Three-Dimensional Element of Cable Implementation in 20sim.....	43
Figure 6.1. Modal Testing over Bar and Cable.....	45
Figure 6.2. Experimental Set-Up for Cable and Pole Model Verification (Pinto & Rideout, 2016)	46
Figure 6.3. Schematic of Time Series Tests	47

Figure 6.4. Schematics of the Bar Configurations for Additional Damping	48
Figure 7.1. Acceleration Time Series for Pole Tip, Measurement and Simulation (Pinto & Rideout, 2016).....	50
Figure 7.2. Acceleration Time Series of Cable Tests (Pinto & Rideout, 2016).....	53
Figure 7.3. Acceleration Time Series for the Pole and Cable Connected. (Pinto & Rideout, 2016)	55
Figure 7.4. Experimental Stabilization Chart of the Pole and Cable (Cable Tension 15N) (Pinto & Rideout, 2016).....	56
Figure 7.5. Transfer Function of the Bar, without Damping (Top) and with Damping 2-3 (Bottom), Blue is the Accelerometer at the Tip, Red is the Accelerometer at Mid-way..	57
Figure 7.6. Variations in Bar Damping – Before and After Damping Increase	58
Figure 7.7. Transfer Function of the Bar and Cable, without Damping (top) and with Damping 2-3 (bottom), Blue is the Accelerometer at the Tip, Red is the Accelerometer at Mid-way	59
Figure 7.8. Variations in Bar/Cable Damping – Before and After Damping Increase	60

List of Symbols and Abbreviations

A	Area of the section of the cable/beam, m^2 .
k_e	Elastic constant of the cable, N/m .
n	Number of elements/modes used in the model.
b_e	Element damping of the cable, $N\text{-s}/m$.
b_{critic}	Critic damping of the cable, $N\text{-s}/m$.
E	Elastic modulus, N/m^2 .
F	Axial force of the cable, or lateral force on the beam, N .
F_x	Force in the horizontal x direction, N .
F_y	Force in the vertical y direction, N .
F_z	Force in the z direction, N .
F_b	Force in the cable dashpot, N .
F_s	Spring force of the cable, N .
f	Function of time for separation of variables.
f_n	Natural frequency of a string, Hz .
l_e	Total length of the cable divided by n elements, m .
\dot{l}_e	Rate of change of element length, m/s .
ζ	Damping factor of the cable, dimensionless.
m_e	Mass of the element of cable, kg .
μ	Linear density of the cable, Kg/m .
δ	Dirac delta.
δ_e	Deformation of the element of cable, m .

$\dot{\delta}_e$	Velocity of cable element deformation, m/s.
θ_e	Angle between cable and the horizontal direction, radians.
α_e	Angle between cable and the x direction, radians.
β_e	Angle between cable and the y direction, radians.
γ_e	Angle between cable and the z direction, radians.
$x_{1,2}$	Displacement (x) of left/right element ends, m.
$y_{1,2}$	Displacement (y) of left/right element ends, m.
w	Lateral beam displacement, m.
I	Area moment of inertia for the beam, m ⁴ .
Y	Mode shape functions.
ω	Mode frequency, rad/s.
$\beta_n l$	Weighted frequency.
l	Length of the beam, m.
m_n	Modal mass of the beam.
k_n	Modal stiffness of the beam
ρ	Density, kg/m ³ .
T	Cable tension, N.
L	Length of the cable/beam, m.
ε_i	Damping ratio.
ω_n	Natural frequencies, rad/s.
ω_i	Modal frequency measured, Hz.
m_i	Modal mass for the beam model, kg.

m_i	Mass of the element for the cable model, kg.
a_x	Acceleration of the cable mass in the x direction, m/s ² .
a_y	Acceleration of the cable mass in the y direction, m/s ² .
g	Gravity acceleration, m/s ² .
μ	Linear density of the cable, kg/m.
T	Tension over the cable, N.
FRF	Frequency response function.
DAQ	Data acquisition system.
FEA	Finite element analysis.
DFFT	Discrete fast Fourier transform.
DOF	Degree of freedom.

List of Appendices

Appendix A.....70

Appendix B.....72

Appendix C.....75

Appendix D.....77

Chapter 1 - Introduction

The use of wooden poles goes back to the end of the 19th century when the earliest telegraphic lines were installed for communication and, later, with the implementation of public electrification. Wood was an obvious choice of material for this purpose, since initial attempts to make underground lines failed at the time, and wood is abundant, resilient and durable. These characteristics gave the wooden pole the usage preference throughout the centuries and they are still widely used all over North America, where about 130 million poles are currently in use (Wood Poles, 2016). In Newfoundland, NL Hydro maintains 26000 wooden poles for electrical transmission lines (Dillon, 2009).

Wooden poles are not only abundant and relatively inexpensive, but they also present several advantages when compared with steel or concrete poles. They have lower storage costs and don't require protection for transportation. The amount of space necessary to stack wooden poles is less than half of the needed for steel and concrete poles, according to the manufacturers (Scan Pole, 2016). When compared with concrete and steel poles, wooden poles can resist surface impacts better due to their elastic characteristics. Impacts can cause cracks over concrete allowing for water infiltration and damage propagation. Superficial damages also affect the durability of steel poles, since damages in the coating can favour rust. Besides, wood has a great ratio between strength and weight, presents excellent dielectric characteristics and has a life expectancy of between 35 to 50 years when subjected to proper treatment and maintenance (Morrell, 2016).

However, during its life span, wooden poles are subjected to environmental conditions that cause degradation of the material. Insect infestation, animal perforations, plant and fungi growth, weather variations, etc., all contribute to the deterioration of the wooden pole. With time, these factors compromise the network reliability, the safety of the population and the operators of the electrical system. Pole strength degradation is a serious issue, causing the industry to invest considerable amounts of money in maintenance programs and research. NL Hydro, for example, presents online reports which show that in 2017, investments of 3.8 million Canadian dollars will be expended on pole maintenance and upgrades (Hiller, 2016).

Research Proposal

This research is a continuation of work performed by NL Hydro and Memorial University of Newfoundland with the aim of studying the use of non-destructive tests to assess wooden utility pole integrity. Previous researchers started with initiatives a few years ago, to provide information showing a correlation between modal damping and pole strength when the poles are excited by a hit of a hammer in a laboratory (non-destructive testing). The tests using the modal technique appeared to be more accurate than other non-destructive methods used by NL Hydro, based on the experience of the author's research group.

New investigations have been carried out since then, and the most recent research stage obtained information through field measurements. The first results from that research indicate that modal test quality decreases in the field, presumably due to foundation

damping and compliance, cables, or a combination of both effects (Rideout & Whelan, 2014).

Now, to give continuity to this research, it is necessary to better understand how cables interact with poles, and to determine whether it is possible to find a pattern that could help improve the existing model in order to obtain better strength predictions for wooden poles. Overall, this research proposes to implement and validate reliable models for the dynamic simulation of pole interaction with cables. The model should predict dynamic cable tension and motion, cable natural frequencies and damping ratios, pole motion, and pole modal properties during simulated modal testing.

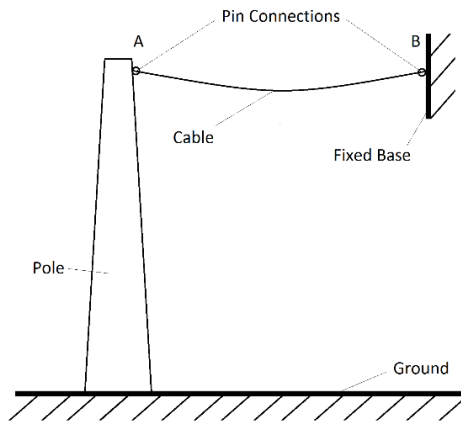


Figure 1.1. Schematics of Pole - Cable System (Pinto & Rideout, 2016)

In addition, other research objectives are to design a reduced physical model of a pole and a cable that can be used for model validation and for experimental tests that are performed to bring insights to system behaviour. Figure 1.1 presents a schematic of the pole-cable system proposed for this study.

The bond graph formalism is used for implementation of pole and cable models due to its modular characteristics, allowing easy changes in each sub-model.

Presently, work is being performed to validate computational models which simulate the diverse *in-situ* configurations of wooden poles (i.e. with attachments such as conductors, isolators or guy cables). This approach provides a better estimate for future statistical models. It is expected that this research will result in a method for *in-situ* verification of the quality of wooden poles through modal testing associated with statistical analysis of the empirical results.

This work is organized in eight chapters which systematically present the research done, and offers new contributions towards the overall development of wooden pole test methods. Chapter 2, Literature Review, is a comprehensive synthesis of some of the relevant research done so far on NDT for wood and wooden poles, and on the modeling of the dynamic behaviour of cables. In Chapter 3, a theoretical background on the mathematical and engineering resources used in this work is presented. Chapter 4 introduces pole theoretical and physical models developed along with design guidelines for a reduced physical pole model. Chapter 5 presents the development of cable models and a reduced scale cable. Chapter 6 presents proposed tests for verification of the created models. Chapter 7 presents results and discussions regarding physical and simulated models. Finally, Chapter 8 presents the conclusions on the results and proposes future research directions related to these topics.

Chapter 2 - Literature Review

Non-destructive Methods

As a natural material extracted from forests, wood cannot be manufactured with strict quality patterns in the same way metals, ceramics and composites, for example, can be. Wood presents specific characteristics such as knots, cross grains, checks, splits, and a rigorous selection is necessary to obtain the best samples for engineering applications. In addition, wood deteriorates and suffer from the attack of insects, fungi and the weather even when treated (Forest Products Laboratory, 1999). For these reasons, there is considerable interest in developing and improving the existing non-destructive test (NDT) methods to assess wood properties, both during processing and along its entire life span. In this work, our interest is specifically related to the use NDT for wooden utility poles. However, a brief review of the main techniques used and an overview of the previous research of this group are first presented.

Non-destructive methods for testing and structural assessment can be defined, according to Ross (1991), as the science that allows the identification of mechanical properties of materials without causing structural damage or harming their final application. Thus, non-destructive techniques used for testing wood have a clear advantage: the studied sample is not damaged. However, it is particularly difficult to apply the methods to wood due to its orthotropic characteristics or due to the diverse configurations the installed material can assume. Diverse studies and methods were developed to attempt to explore ways for the non-destructive identification of wood properties.

Ross (1991), for example, presents in his review some of the NDT techniques that have been used for wood testing by many researchers, such as: bending techniques, transverse vibrations, and stress wave techniques. Ross also presents very briefly some other techniques such as: ultrasonic waves, attenuation of x-rays methods, visual inspection (not a quantitative method), screw withdrawal and pick (causing some small damage), and high speed puncture.

From the list above, Ross (1991) highlighted three methods: First, the static bending technique, which uses measurable properties of the material along with static bending theory to obtain the sample modulus of elasticity. One example of how this method works can be given by considering the lumber as a cantilever beam, and test its deformation under controlled applied loads. The elastic relationship between displacement and applied load, along with beam theory, should suffice to estimate the elastic modulus of the lumber. The second method, transverse vibration, uses the dynamic characteristics of lumber to determine the modulus of elasticity, measuring the resonant frequencies and matching them with equations for free beam vibration, for example. Lastly, stress wave techniques are performed by exciting the lumber to cause vibrations and then monitoring the velocity of the resulting sound propagating through the material, to permit a comparison of the results with experimental tables that correlate velocity and elastic modulus. The author concludes his review by considering that, despite the value of the other methods, stress wave techniques should be studied more because they appear to offer promising possibilities with low equipment cost and because, up to that moment, there were no study on how the boundary conditions of diverse wood structures would affect measurements verified in the laboratory.

Despite the extensive work done with NDT for wood testing, application of the methods for wooden poles is more recent. Usually a combination of methods has been used by utility companies to test their networks. A common combination for testing wooden poles is a visual inspection, where a technician climbs and observes the pole looking for critical damage, and sound inspection, where an experienced technician climbs the pole while striking its surface with a hammer and listening to the sound. Sounds that are contained and not reverberating may indicate rotten areas. Both methods are clearly very subjective techniques, depending greatly on the experience of the technician, and are usually used with a more quantitative method such as the use of a resistograph or a vibration appraisal (Datla & Pandey, 2006).

Bodig & Phillips (1984) report the application of a non-destructive method developed by other researchers that uses the speed of sound waves propagating along a pole. Sound velocity is measured at one foot above the ground line, and registered with a timer. The researchers correlated these measurements with the bending strength at the ground line of the wooden poles, revealing bad correlations. However, when they applied collected data and associated it with statistical models developed by other authors, they were able to create a strong statistical strength distribution for the poles.

Another non-destructive method that makes use of vibration techniques for testing utility poles was proposed by (Tallavo, Cascante, & Pandey, 2012). Their work presents the use of ultrasonic waves, along with other identification parameters for use in cylindrical and orthotropic materials. Instead of estimating the modulus of elasticity of the wood by comparing the velocity of the ultrasonic waves in the medium with experimental tables for different species, the authors consider wave velocity along with the transmission factor and

the module of elasticity in radial and tangential directions (calculated for specific temperatures and moisture content). The apparatus uses a “belt” of five receivers and four ultrasonic transmitters around an investigated section of pole. Additional parameters associated with statistical indices allow an estimation of wood quality. Sound poles and old poles were tested with this method, and areas of deterioration were identified in the old poles. Though the method presented good results, it can only predict defects on the section of the pole that is being investigated, creating difficulties for *in-situ* lengthwise testing.

Downer, (2010), whose work is a precursor to the present research, introduced a new approach to verify wooden pole quality. In his work, the design of experiments (DOE) technique associated with experimental modal testing identification (for frequency and damping ratios) was used to locate defects in wooden poles. DOE was used for the creation of regression models that would be able to predict defects based on the dynamic response of the wooden pole for frequency and damping ratio. Downer also found good correlation between modal damping and pole strength in laboratorial tests. However, this correlation became weakened when used with data collected in field. The discrepancy was attributed to the different foundation of the poles and to the conductors connected to the poles.

Therefore, to investigate how these processes occur in field, virtual simulated models are necessary, allowing to isolate the parameters of interest and improving the correlations.

Background for Cable Modeling Theory, Experiments and Simulation

The relevance of modeling cable dynamics is well known in civil applications such as suspended bridges, guy-cables for masts, poles, communication towers, antennas, structural tents, and precision structures (such as those used in space). One famous example of dynamic effects on cables for civil applications, which is constantly cited in diverse engineering and physics textbooks, was the collapse of the Tacoma Narrows Bridge in Washington, U.S.A. The bridge collapsed due to self-excited vibrations resulting from an interaction between fluid and the structure caused by wind conditions. This was a tragic example of how dynamic behaviour can affect such cable structures (Billah & Scanlan, 1991).

Despite that, cable dynamics involving electricity transmission lines have been studied mainly because of the possibility that induced vibrations can damage the circuits and structures, the vibrations in this case being caused by winds shedding over the cable.

Starossek (1994), in his review of cable dynamics, presents the history and the state of art of cable theory. Cable dynamics studies have been done since the beginning of modern mechanics and mathematics, but new applications and materials require new developments in modeling and cable theory. Starossek's review presents different attempted approaches. By introducing simplifications to the model, such as considering the cable as a massless string that is inextensible and fixed at two levered ends with no sag; and by adding weights along the string in an attempt to discretize the problem. Only by the end of the 19th century were there enough contributions to describe the motion and frequency of wires with no sag,

to set out the discreet approach for sagging wires, and to identify empirical equations for sagging cables. The author explains that before the 1970s there was no theory or experiment to solve the problem of comparing the frequencies of a cable with no sag with the frequencies of a taut string. Later, researchers found that it was necessary to include cable elasticity to the equation, assuming cable dynamic tension as a function of time alone. In addition, the author presents the development of a linear theory for cables with small sags.

Another approach for cable modeling is to consider a multi-stranded cable as a shear beam model, and then adjust the parameters such as area, density, elastic modulus, shear rigidity, and shear modulus according to measurements of an actual cable (Spak, Agnes, & Inman, 2014). Those researchers were able to rewrite the equation of motion for a beam by modifying the individual parameters and adding shear effect, tension, rotational stiffness, and damping. The authors also performed dynamic tests to verify the model, using four different configurations of cable strands, comparing their experimental results with modeled results for a few modes of vibration. In addition to developing the cable model, the authors noticed that the common boundary conditions used for beams, such as pinned or clamped at both extremities, would not be consistent with the experimental setup available. To address this problem, the authors added rotational and translational springs at the extremities of the cable model, and this produced better results when compared with data from the experiments. Their study, which intended to generate dynamic cable models for studies on precision applications in space, presented excellent results in comparisons between the model and the experiments. The authors concluded that the model alone is able to predict well only the first three modes and better results are obtained for thicker cables.

They also obtained improved results by adding rotational and linear springs to the model, as boundary conditions at the cable extremities.

The cable model presented by Spak et al. (2014) was successfully used as a simple and effective tool to describe cables with little or no sag. The beam model cable was also used for modeling electrical transmission line dynamics. A simplified version of the beam model was presented by Barbieri et al. (2004). They studied the dynamic behaviour of transmission lines, aiming to improve models used in new projects and maintenance. For this project, finite element analysis is used with the mathematical beam model and verified through experimental and theoretical results, and the cables were kept tensioned at 5% of the rated tensile strength (10 KN).

Another part of this project involved verification of the models by means of experimentation, so it is relevant to question how to perform a dynamic test on a cable that would allow the identification of its resonant frequencies and modal damping. Qiu & Maji (2011) experimented with cables made of steel and carbon fiber. They built a wood setup that was similar to a rectangular frame, where they could attach one extremity of the cable to a load cell while leaving the other side fixed. They installed two accelerometers over the cable in strategic positions to avoid the nodal points and excited it in the center, measuring the accelerations for diverse levels of tension. The measured time series of acceleration was investigated using Fast Fourier Transformation (FFT) of computational commercial tools, and the damping was calculated using the half-power bandwidth technique. The authors compared their results with the theory for inextensible strings (presented later in Chapter 5) and concluded that a reduction in tension over the cable causes an increase in

vibration frequency, while frequency decreases when the number of twists on the carbon fiber are increased and damping decreases with an increase in tension.

It is also possible to obtain dynamic parameters from transmission lines by measuring the frequency response function (FRF) from a known excitation. This method can be executed with modal analysis, using a hammer as the excitation source and accelerometers as the means to acquire the responses. The generated FRF makes it possible to obtain the modal damping and frequencies. This information can be used to feed diverse types of dynamic cable models, such as lumped segmentation models, parametric models or finite element models, as seen in Barbieri et al. (2004).

For the cable simulations for this project, the lumped segmentation model presented itself as a convenient way to represent cable response in the analysis of an *in-situ* wooden pole. This approach is intuitive since it consists of a sort of discretization of the system in terms of known linear components. In the cable case, it is assumed that it can be divided into a finite number of segments, each one containing a spring, a damper and a mass. Although the lumped segmentation model is simple to elaborate and visualize, the more one increases the number of lumps, the more difficult it becomes to achieve convergence. In addition, low frequencies can be improved with an increase in the number of lumps, although this also produces spurious results in the high frequency range (Karnopp, Margolis & Rosenberg, 2012).

The dynamic modeling of a wire as a lumped segment can be found in Skjong & Pedersen (2016). Using a bond graph to simulate a hydraulic winch system for sub-sea applications, the authors created a winch configuration that included the wire, the reel and the payload. This work is based on their approach, modeling an electric cable as lumped segments of

wire (with mass, spring and damping) moving in two dimensions in the same way as presented by Skjong & Pedersen (2014), with the main contribution being an extension of their work for the three-dimensional world.

Chapter 3 - Research Methods

This chapter presents a brief introduction to the theoretical background of the engineering resources used in this work. Bond graph formalism is introduced with a simple example using a single degree of freedom oscillator. Information on modal testing and experimental modal analysis is presented, along with some of the methods used to acquire signals. This text does not intend to go deeper into mathematical explanations for each method, since much more complete literature is available and cited for reader investigation.

Bond Graphs

Bond graph formalism was developed by Henry Paynter to facilitate the modeling and integration of dynamic systems that are usually composed of elements in multidisciplinary fields. It derives from the fact that interaction between various fields (electrical, mechanical, hydraulic systems, etc.) is an exchange of energy and information in their diverse forms. Bond graph representation reduces the complexity of each subsystem (even ones in different fields) by allowing the creation of systems through an association of ideal elements connected by power bonds. This approach is elegant since the apparent complexity imposed by physical boundaries between areas vanishes, leaving only power interactions which are easily visualized after some practice.

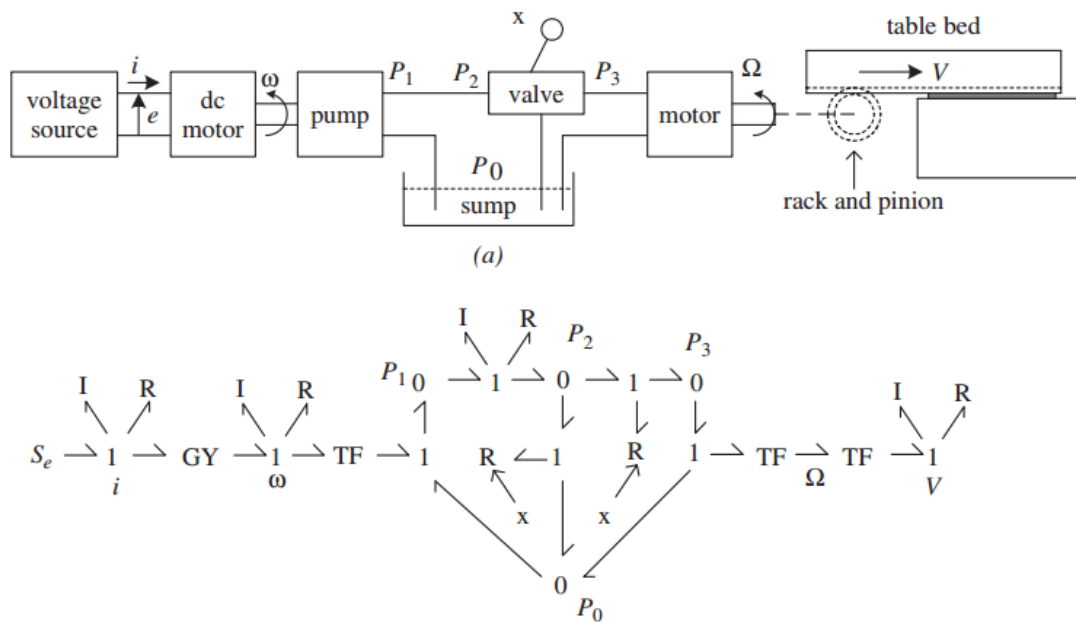


Figure 3.1. Bond Graph of a Generic System and its Elements (Extracted from Karnopp, et al. (2012))

Figure 3.1 shows an electrical – mechanical system modeled using graph elements such as power bonds, junctions (1-junction and 0-junction), resistors (R), compliance (C), inertia (I), transformers (TF), and sources (flow and effort). Here, power bonds are half arrows representing the conduction of power (flow and effort) between junctions and components. The bonds have strokes assigned to their tails or arrows to emphasize the direction of the flow and to help to determine which variables are dependent or independent when writing the model equations. The 1-junctions', analog to an electrical loop, allow the same flow in all connected ports, with the sum of efforts resulting in zero. 0-junctions' exhibit a complementary behaviour with 1-junctions', efforts in all connected ports are the same, and the sum of flows is zero, analog to Kirchhoff's current law. Other basic components are: Resistors or dissipative elements where energy is released from the system to the

environment, analog to electrical resistances or viscosity dampers; Capacitors or storage elements, which represent accumulators of energy, analog to electrical capacitors or mechanical springs; Inertia elements, which also are storage elements analog to electrical inductances; and Transformers, elements that are able to conserve power entering and leaving them, similar to an electrical transformer or a mechanical lever. All elements obey a set of rules having equations describing their behaviour, as seen in more detail in Karnopp, et al. (2012).

Note that the element terminologies resemble the electrical world but are not intended only for electrical modeling, due to the analog behaviour between elements in different fields. For example, an (R) symbol could be used to represent a valve on a hydraulic circuit and a (C) symbol could be used to represent a spring in a mechanical scheme.

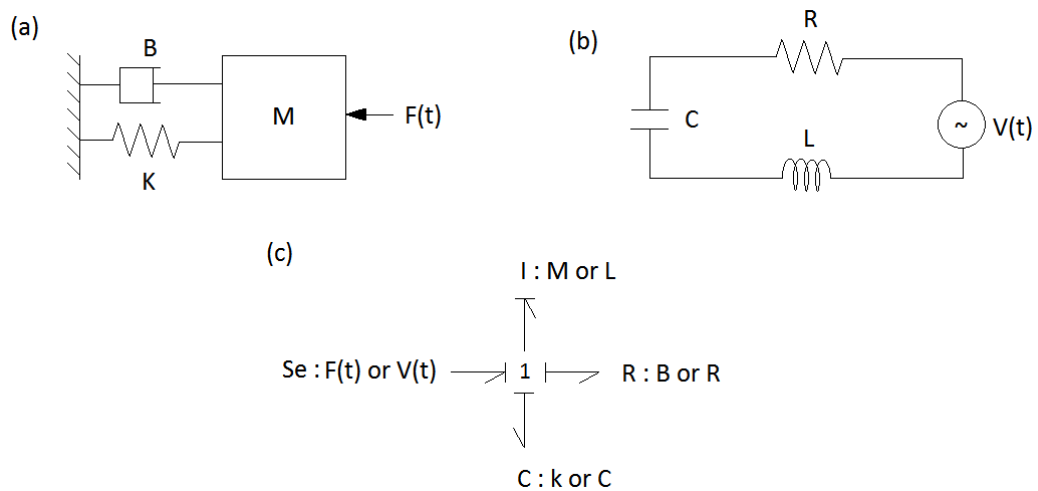


Figure 3.2. Mechanical and Electrical Systems in Bond Graph Representation

Figure 3.2(c) illustrates an example where the same bond graph is used to represent two different fields: the mass, spring and damper presented in Figure 3.2(a) is a model of a

linear oscillator with one degree of freedom. Figure 3.2(b) shows an electric circuit containing an electrical resistance, a capacitor and an inductor connected to a source of variable voltage.

In conclusion, the bond graph is a methodical tool for modeling dynamic systems to allow integration between fields and facilitate the derivation of governing equations. From the time of the development of Bond graph formalism, one would solve derived equations using math or, depending on the complexity of the problem, some numerical integration method. The models derived in this project are implemented using commercial software called *20sim* (2015). This software has a graphical interface specifically designed for drawing bond graph schematics, offering a library of components and diverse resources for simulation and animation. In addition, *20sim* (2015) has a sophisticated suite of integrators and a rich Frequency Domain toolbox for eigenvalues calculations.

Modal Testing

Mechanical structures may vibrate due to diverse operational situations and external excitation. If, for example, the component is a structural part of a machine it will probably experience vibrations throughout its lifespan due to moving shafts, pumps, motors, engines, gears and other dynamic devices. If the component is part of a static structure, a bridge for example, it might be subject to vibration by external sources of excitation, such as wind, and vehicles and people passing over it. In both scenarios, the vibrations, inherent or causal, may degrade the structure or even trigger a destructive effect.

Realization of these phenomena has led researchers to the development of mathematical and experimental tools to investigate structural dynamic response. Thus, a technique called modal analysis was investigated by the aerospace industry beginning in the 1940's, for the dynamic evaluation of aircraft. Since then, the technique has evolved and the use of modal analysis now has broad applications in the industry: it can be used for the development of analytical dynamic models, for structural damage detection, for certification, and for design modification (Ewins, 2000).

The next sections in this chapter offer a general overview on how to perform and analyse impact modal testing.

Performing a Modal Test

Experimental modal analysis is a system identification method used to obtain the natural frequencies, mode shapes and damping of structures, by analysing the transfer function spectrum resulting from measured vibrations that are caused by known excitation. In other words, experimental modal analysis makes it possible to extract useful dynamic information from structural vibration responses when exciting the structure properly. The information collected can be used for modeling dynamic structures, employing methods such as variable separation or finite element analysis (FEA). It also has been applied to the non-destructive testing of the structural integrity of wood (as explained in Downer (2010)). Many different methods have been developed to execute an experimental modal analysis, as can be seen in details in Ewins (2000). In this work, a technique called impact or hammer

excitation is used, which consists of exciting the structure using a special hammer containing a load cell on its tip. The vibrational response is measured through accelerometers placed at known locations along the analysed part. Figure 3.3 shows a schematic of a generic impact modal test.

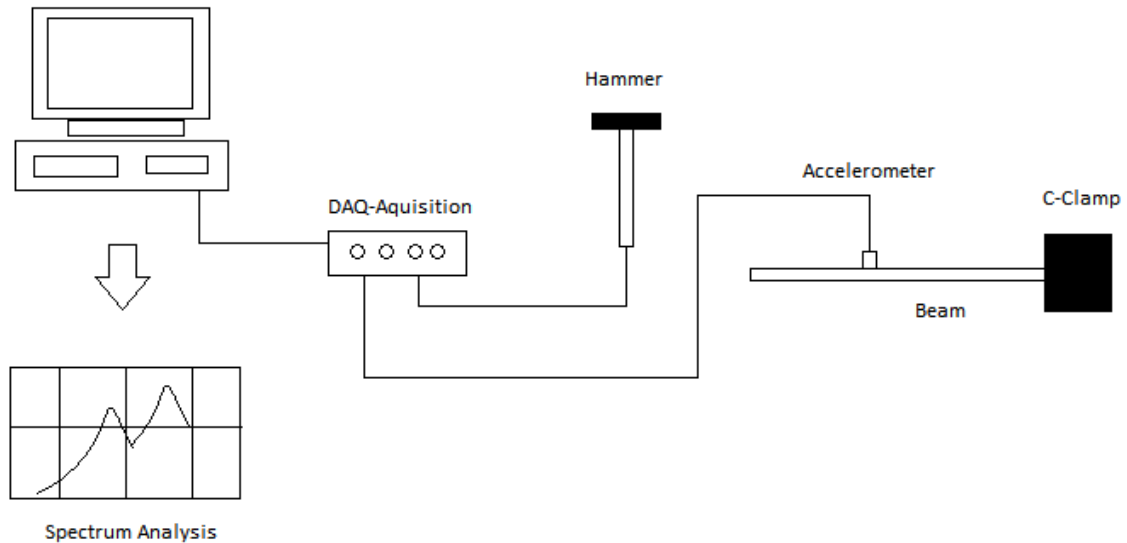


Figure 3.3. Schematics of a Generic Modal Test of a Beam Using Hammer Excitation

The sensors, accelerometers and load cell on the hammer produce a small but measurable analog electrical current that is filtered, amplified and sampled for digital processing. This is usually done by a data acquisition system (DAQ), which is an electronic device that samples and digitizes the signals streaming them to a personal computer where the analysis can proceed. Here, the analyses that follow are obtained using FRFs measured by the equipment presented in Table 3.1. More information on the hammer, accelerometer, DAQ and load cell, can be found in the Appendices A, B, C and D.

Table 3.1. Equipment for Modal Testing and Tension Measurements

<i>Equipment</i>	<i>Manufacturer</i>	<i>Model</i>
<i>Impact Hammer</i>	Bruel & Kjaer	8205-002
<i>Accelerometer</i>	Bruel & Kjaer	4507 B 004
<i>DAQ</i>	National Instruments	NI USB-4432
<i>Data cables</i>	PCB	
<i>Software for Analysis</i>	ModalVIEW	
<i>S-Beam Load Cell</i>	Omega	LCCA-250 250-lb

The load cell is not part of the modal testing. However, as seen in the literature review, the natural frequencies of cables vary depending on the tension on the cable, thus, tension is registered for some of the tests proposed in Chapter 6.

In this project, the software ModalVIEW (2012) will be used to extract modal information, frequency and damping. ModalVIEW (2012) provides a complete low-cost tool for modal testing and analysis. The software has a main project management interface divided in several icons where it is possible to: acquire data, model 3D geometric drawings, create animations, and perform modal analysis with multiple degrees of freedom polynomial curve fitting.

Thus, after performing the measurements, the resulting time series signal is then multiplied by a “window” function which causes the amplitude of the data to be zero at the beginning and end of the recording, closing the sequence in a recognizable period. Windowing is a pre-processing method necessary to avoid “leakage” when the FRF is subjected to the discrete fast Fourier transform (DFFT), which is the next step in the analysis. Leakage will occur when the alternative signal does not have an integer number of periods, causing the

(DFFT) to create high frequency components that are not present in the original signal. A detailed explanation of data acquisition systems and how to avoid leakage can be found in Figliola & Beastley (2011).

General modal testing extraction is used to obtain all modal parameters (modal shapes, frequency and damping ratio). However, for this project we will only be interested in modal frequency and damping because, as previous presented, researchers in this group found correlations between those parameters and wood decay.

Using ModalVIEW (2012), an averaging method is employed to remove noise, improving the FRF results and permitting the analysis to proceed using different methods.

In ModalVIEW (2012), an averaging method is used to remove noise improving the results of the FRFs and the analysis can proceed with different methods.

ModalVIEW (2012) also provides a tool called stabilization chart to perform modal extraction. This tool can help the analyst to find real physical poles from the mathematical ones created, due to the presence of noise on the acquired signal. After choosing a frequency interval to investigate, the analyst can indicate the maximum model order for the polynomial that will be used for curve fitting the FRFs. Then a chart is created with the poles calculated from the model, increasing the order up to the maximum previously selected. The stable poles, which have a corresponding negative real part and are stable for frequency, damping ratio and mode shape, receive in ModalVIEW a green “s” on the chart. Other codes are attributed to identify the quality of the estimation; v, d, f, and o, and more details for these codes can be seen in ModalVIEW’s help content. Relevant poles that can be associated to physical modes appear in the chart forming a straight, or almost straight,

vertical line, and mathematical poles usually appear scattered about without a relevant pattern.

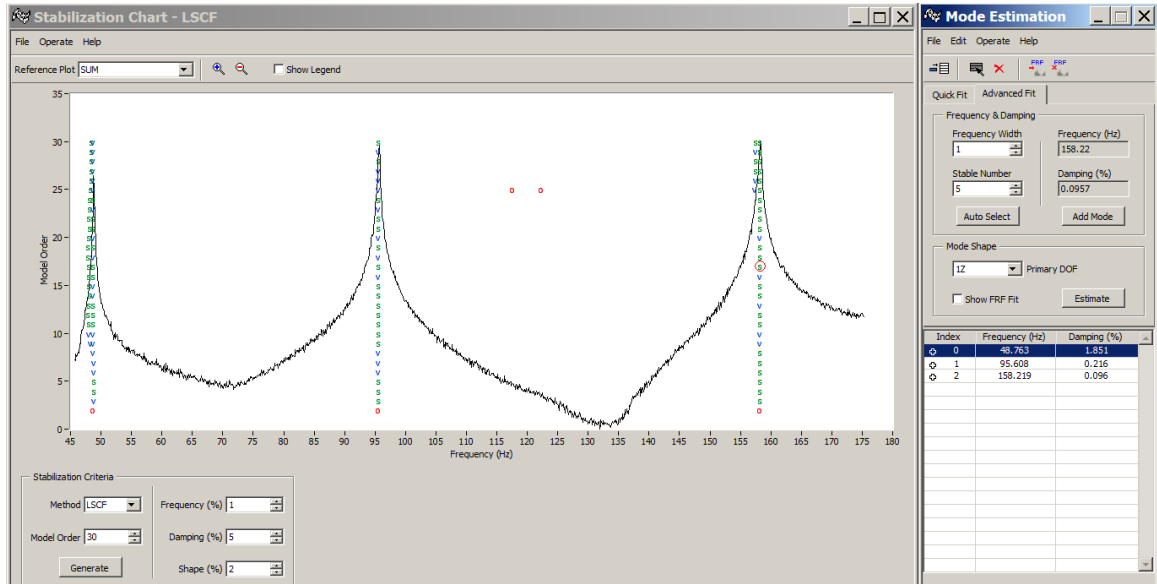


Figure 3.4. Generic Stabilization Chart Analysis Generated with ModalVIEW

Figure 3.4 presents an analysis performed for the FRF response of a vibrating bar, considering frequencies of 45 to 180 Hz. Three modes are observed: each has stable modes lined up in the same frequency, with an increase in model order. Selecting any of the stable values causes them to appear on the right side of the window with a numerical estimation of the frequency and damping ratio.

Chapter 4 - Pole Modeling

In this chapter, a dynamic pole model is developed through the application of the theory for vibrating beams along with assumptions about the material, geometry, and boundary conditions. Although this project aims to produce information for use in future developments on wooden pole non-destructive testing, no wood pieces or wooden properties will be used here. Instead, a theoretical and numerical model of a cantilever beam is explored by using bond graph representation and a physical beam is designed allowing verification tests of the numerical model.

Modeling an Euler-Bernoulli Beam through Distributed Parameters

The most common mathematical models used for beams are the Euler- Bernoulli and the Timoshenko models. The difference between the models rests upon the sort of assumptions made to establish the equations of motion. The Euler-Bernoulli model assumes that any plane perpendicular to the neutral axis before bending will remain plane after deformation. The Timoshenko beam model, on the other hand, accounts for the shear deformation and rotational bending effects, allowing the deformation of the sections perpendicular to the neutral axis. Thus, the Euler-Bernoulli beam is stiffer and presents less deformation under static load than the Timoshenko beam. However, the difference between models is minimal unless when working with stubby beams and large deformation, when Timoshenko's model is recommended. For dynamic loads, the addition of rotational inertia in

Timoshenko's model produce better results in high frequencies. In addition, Inman (2014) affirms that the assumption of small shear deformation in Euler-Bernoulli beams can be used when the ratio between the length and the thickness and the ratio between the length and the depth of the beam is greater than ten.

Because the Euler-Bernoulli model is simpler but presents good results for the range of frequencies expected in the experiments (bellow 200 Hz), it will be used here and introduced as presented by Inman (2014) and Karnopp, et al. (2012), for a beam subjected to small deflection.

In the following equations, the geometric section of the beam is considered constant, although future work might use the model of a tapered pole presented by Rideout & Whelan (2014). In that work, the authors consider the differences in the resulting modal shapes between the pole model with regular and tapered sections.

Thus, Equation 4.1 represents the transverse displacement for a beam modeled as an Euler-Bernoulli beam with constant sectional area acted on by a force that varies over time:

$$EI \frac{\partial^4 w}{\partial x^4} + \rho A \frac{\partial^2 w}{\partial t^2} = F(x, t) \quad (4.1)$$

Through the assumption of separations of variables, it is possible to write the vertical displacement $w(x, t)$ as the product of a displacement function $Y(x)$ by a time function $f(t)$, such as,

$$w(x, t) = Y(x)f(t) \quad (4.2)$$

substituting Equation 4.2 into Equation 4.1 and solving for the homogeneous form, results in,

$$\frac{EI}{Y\rho A} \frac{d^4 Y}{dx^4} + \frac{1}{f} \frac{d^2 f}{dt^2} = 0 \quad (4.3)$$

Now, replacing the second term on the left-hand side of Equation 4.3 with ω^2 , we can write the motion equation as,

$$\frac{d^4 Y}{dx^4} + \frac{\rho A}{EI} Y \omega^2 = 0 \quad (4.4)$$

and Equation 4.4 has a general solution of the form,

$$Y(x) = \sin(\beta x) a_1 + \cos(\beta x) a_2 + \sinh(\beta x) a_3 + \cosh(\beta x) a_4 \quad (4.5)$$

Because we want to model a cantilever beam, it is necessary to apply the four boundary conditions to the general solution of Equation 4.5: Bending moment and shear force are zero at the beam's free extremity, and the deflection and slope are zero at the clamped extremity:

$$EI \frac{\partial^2 w}{\partial x^2} = EI \frac{\partial^4 w}{\partial x^4} = 0$$

$$w(x, t) = \frac{\partial w}{\partial x} = 0$$

When substituted into Equation 4.5, this results in a system of four equations and four unknowns (a_1, a_2, a_3, a_4),

$$\begin{bmatrix} \beta & 0 & \beta & 0 \\ 0 & 1 & 0 & 1 \\ -\beta^2 \sin(L\beta) & -\beta^2 \cos(L\beta) & \beta^2 \sinh(L\beta) & \beta^2 \cosh(L\beta) \\ -\beta^3 \cos(L\beta) & \beta^3 \sin(L\beta) & \beta^3 \cosh(L\beta) & \beta^3 \sinh(L\beta) \end{bmatrix} \begin{Bmatrix} a_1 \\ a_2 \\ a_3 \\ a_4 \end{Bmatrix} = \begin{Bmatrix} 0 \\ 0 \\ 0 \\ 0 \end{Bmatrix} \quad (4.6)$$

Making the determinant of Equation 4.6 equal zero results in the characteristic equation,

$$\cos(\beta l) \cosh(\beta l) = -1 \quad (4.7)$$

The quantity βl is called “weighted frequencies” and can have infinite solutions depending on the value choices for β . Solving Equation 4.7 yields the following solutions (Inman, 2014).

$$\begin{aligned}\beta_1 l &= 3.926602 & \beta_2 l &= 7.068583 \\ \beta_3 l &= 10.210176 & \beta_4 l &= 13.351768 \\ \beta_5 l &= 16.49336143\end{aligned}$$

Values greater than $n = 5$ are well approximated by,

$$\beta_n l = \frac{(4n + 1)\pi}{4} \quad (4.8)$$

and the natural frequencies of the system can be determined by

$$\omega_n = \beta_n^2 \sqrt{\frac{EI}{\rho A}} \quad (4.9)$$

In addition, the solution of Equation 4.5 leads to the mode shapes (eigenfunctions) equation,

$$Y = \frac{\sinh(\beta l) - \sin(\beta l)}{\cosh(\beta l) + \cos(\beta l)} (\sin(\beta x) - \sinh(\beta x)) + \cosh(\beta x) - \cos(\beta x) \quad (4.10)$$

Where x , is the position along the beam.

Bond Graph Implementation of an Euler-Beam (Modal Expansion)

The cantilever beam derived in the previous section through the assumption of separation of variables can be adapted to the bond graph representation for use in computational

simulations. Karnopp, et al. (2012) presents the adaptation of the equations above in a more suitable form to be used in a bond graph model of the Euler-Bernoulli beam.

It starts by rewriting the total response function (Equation 4.2). Linearity allows the total response $Y_n(x)$ to be written as an infinite summation of the mode shapes multiplied by the modal time responses, such as,

$$w(x, t) = \sum_{n=1}^{\infty} Y_n(x) f_n(t) \quad (4.11)$$

Now, following the idea introduced in the previous section, we can insert Equation 4.11 into a modified form of Equation 4.2. The Dirac delta function is added to incorporate the external point force at the free extremity of the beam. Multiplication by the m^{th} mode shape (Y_m) and integration along the length of the beam results in,

$$\sum_n \left(\int_0^L \rho A Y_n^2 dx \right) \ddot{f}_n + \sum_n \left(\int_0^L \rho A Y_n^2 dx \right) \omega_n^2 f_n = \int_0^L F(t) \delta(x - L) Y_m dx \quad (4.12)$$

With $n = 1, 2, \dots$ and, due to orthogonality, the integrals inside the brackets are equal to zero when $n \neq m$. We are left with an equation that describes the total response of the beam by a summation of infinite second order oscillators.

The integral inside the brackets in the first term is defined as the modal mass and the same term multiplied by the modal frequency squared is defined as the modal stiffness (Karnopp, Margolis & Rosenberg, 2012).

$$m_n = \int_0^L \rho A Y(x)^2 dx, \quad n = 1, 2, \dots \quad (4.13)$$

$$k_n = m_n \omega^2 \quad (4.14)$$

Inserting Equation 4.13 and 4.14 into 4.12 results in the total response:

$$m_n \ddot{f}_n + k_n f_n = F(t) Y_n(x) \quad (4.15)$$

Remembering the introduction to bond graphs presented in Chapter 3, we can use a 1-junction to write the equation of a single degree of freedom oscillator, since it represents a sum of the efforts (force) equal to zero and the same flow (velocity). If we connect to this 1-junction the elements Resistor (R), representing viscous damping, Inertia (I), for the mass, and Compliance (C), or linear spring, we have created a single degree of freedom oscillator.

Up to this moment, there is no damping in our set of equations and, according to Karnopp et al. (2012), separation of variables is only correct without the inclusion of damping. However, because we are assuming that each one of the oscillators acts as a single degree of freedom, the bond graph representation allows us to introduce viscous damping to the Equation 4.15 by using the element Resistor (R) according to,

$$R_i = 2\varepsilon_i \omega_i m_i \quad (4.16)$$

where ε_i is the modal damping ratio extracted from experiments for each mode i .

Now, the equations above can be assembled using the bond graph representation with each one of the oscillators corresponding to a specific mode shape. The difference here is that each element was derived from the general Euler-Bernoulli beam, and Equations 4.13 and 4.14 need to be solved depending on the parameters of the beam and on the frequency of each specific mode.

Having the oscillators, it is necessary to perform a multiplication between the input force at a pre-determined location, and the mode shape at that location, such as that shown in the right side of Equation 4.15. This is done by using transformers (TF) with the modulus equal

Proposing a Physical Model for Testing the Pole Model

To determine what material should be used to represent the pole and serve as the subject of tests for numeric model validation, a theoretical evaluation was performed considering different lengths, material properties, and material availability in our laboratory. In addition, it was established that a metallic bar would be used instead of lumber since this is a preliminary study and because metal properties are constant under similar temperatures, and produce consistent modal testing results.

The condition adopted was to have a bar able to match the lower frequency of the cable. Preliminary tests on the cable alone provided the necessary information for a theoretical trial and error search for the dimensions and material for the bar. Using the available metallic bars and their dimensions, a calculation table was created presenting the theoretical natural frequencies of copper, steel, and brass, considering the dimensions available. Another consideration was to keep the length manageable to allow for comfortable testing. The material that matched the conditions was a copper bar with dimensions: 31.75 x 6.35 mm and free length of 1150.0 mm (the additional length is left for clamping). This bar had its density and elastic modulus estimated by measurements by means of a small sample, and through a bending deflection technique, respectively.

Modifications for Adding Damping

Through the development of this project, further investigations into the possibility of extracting useful dynamic information from the pole, even when it is in the presence of a cable became necessary. The idea proposed is to modify the bar by adding quantified damping without introducing significant changes in mass and frequencies. Two different approaches are explored.

According to Inman (2014), a way of adding damping is by placing layers of materials with damping qualities over the beam. Here, an attempt to add damping by placing one layer of double-sided silicone tape over the length of the bar resulted in no significant change in the frequency or in the damping. Another idea explored was to add damping by using the surrounding atmosphere through aerodynamic drag. In this case, cardboard pieces were added to the bar and modal testing was performed to verify the changes in damping.

Adding damping is relevant since the aim of this test is to verify the possibility of extracting pole dynamic information from the pole and cable system. By comparing the bar alone with the bar and cable connected with and without damping it is possible to visualize the interactions. In Chapter 6, details of the experiments with the cardboard-induced drag are presented. In Chapter 7, the results produced by this approach are presented and discussed.

Chapter 5 - Cable Modeling

This chapter discusses a dynamic cable model that was developed using the lumped-segment technique, which employs several “lumps” of mass interconnected through ideal springs and viscous dampers, creating something similar to a chain. In the modeling, the precise interactions between the wire strands that compose a real cable are ignored.

Instead, we wanted to be able to predict the cable frequency content, with acceptable accuracy, to allow future simulation of a cable’s effects on the pole response spectrum and to study the possibility of extracting useful information about a pole when it is connected to cables. In addition, a short length cable was used during a series of dynamic tests with the scaled pole presented in the previous chapter to verify the developed models.

Lumped-Segmentation Model

Today, people readily understand that everything is made from a combination of small elemental structures. We can “visualize” these structures and even name them: molecules, atoms, particles, electrons, etc. In fact, this ancient idea of small components combining to make bigger systems goes back to the ancient Greek philosophers, and has found well-established grounds in modern science. For most applications, engineers do not need to pursue models which describe fundamental elements down to the atomic scale, but they can explore the idea of combining small components with inherent characteristics to form macro structures.

Even though this idea seems simple and logical, when dealing with dynamic systems, segmentation using small blocks or “lumps” is not easy to implement by “hand” with a pencil. The complexity of the modeling grows the more lumps we add, since each element is associated to an equation. Solving the final equation system would be difficult and time-consuming, and that was why many of these methods were not used until computers became more accessible, with more memory and more processing capacity. Nowadays, computers can solve such equations quickly, allowing the exploration of several techniques for discretization in all areas of science.

Here it is convenient to observe that Inman (2014) suggests the use of the terms “lumped parameter” instead of ‘discrete system’, and “distributed parameters” instead of ‘continuous system’, because the terms are usually employed to refer to the discrete/continuous time domain. Here, “discretization” is related to the division of the system into small lumps that are connected to form a system of equations to describe a motion, and “continuous” is related to the continuity of the function used to describe the motion.

Modeling a Cable through Lumped Segmentation

This derivation is based on the work of Skjong, S., & Pedersen, E. (2016). To illustrate the process of modeling a cable through lumped segmentation, Figure 5.1 is used to show a cable fixed at its extremities. The assumption is that if we could zoom the cable up to a

small division, we would see a chain of masses connected to springs with viscous dampers in parallel.

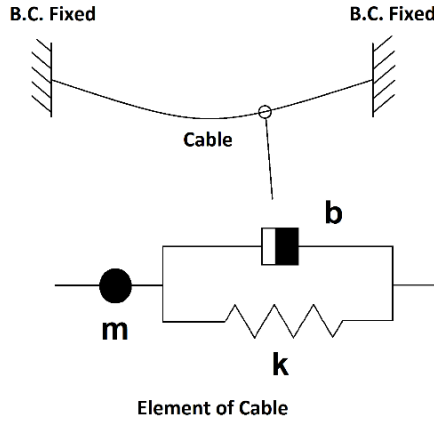


Figure 5.1. Element of Spring (K), Damper (B) and Mass (M) of a Cable (Pinto & Rideout, 2016)

Taking some arbitrary elements of the cable and placing them in a two-dimensional coordinate system allows the visualization of forces in equilibrium, as shown in Figure 5.2.

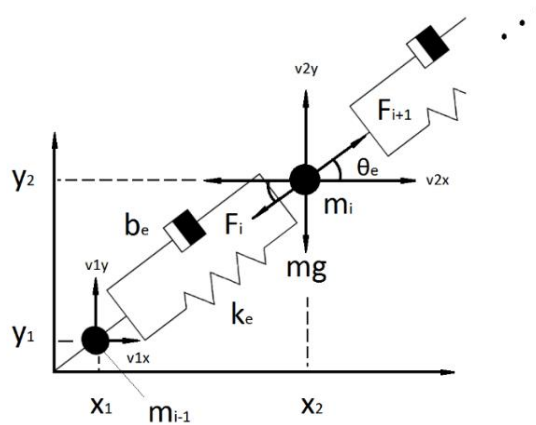


Figure 5.2. Equilibrium of Forces on Two Elements of the Cable on the X-Y Plane (Pinto & Rideout, 2016)

The diagram shows the mass (m_i) surrounded by force components: with the spring/damper on the previous mass (m_{i-1}), due to gravity in the negative y direction and also due to the

next spring/damper elements. The equilibrium requires these forces to balance in the x and y directions:

$$F_x = m_i a_x = 0 \quad (5.1)$$

$$F_y = m_i a_y = m_i g \quad (5.2)$$

To define the forces on the spring and damper we start by presenting relations for each component. The spring is considered linear and massless, with stiffness defined by Equation 5.3 the same way it is for an axial load on a rod.

$$k_e = \frac{EA}{l_e} \quad (5.3)$$

Thus, the spring element with the force given by Equation 5.4 is,

$$F_s = k_e \delta_e \quad (5.4)$$

The damper is modeled with constant viscous damping, according to,

$$F_b = b_e \dot{\delta}_e \quad (5.5)$$

Trigonometry is used to determine the displacement in Equation 5.4, resulting in,

$$\delta_e = \sqrt{(x_2 - x_1)^2 + (y_2 - y_1)^2} - l_e \quad (5.6)$$

Derivative of Equation 5.6 results in the velocity in the axial direction of the spring/damper.

$$\dot{\delta}_e = \frac{2(x_2 - x_1)(\dot{x}_2 - \dot{x}_1) + 2(y_2 - y_1)(\dot{y}_2 - \dot{y}_1)}{2\sqrt{(x_2 - x_1)^2 + (y_2 - y_1)^2}} - \dot{l}_e \quad (5.7)$$

In addition, the angle between the reference plane and the spring/damper elements can be found by the following trigonometric relation,

$$\theta_e = \tan^{-1} \frac{(y_2 - y_1)}{(x_2 - x_1)} \quad (5.8)$$

Now, all equations above can be put together, resulting in the total force from the spring and damper. In addition, the force can be decomposed in the x and y directions.

$$F = F_s + F_b \quad (5.9)$$

$$F_x = F \cos(\theta_e) \quad (5.10)$$

$$F_y = F \sin(\theta_e) \quad (5.11)$$

Bond Graph Implementation of a Cable

The equations describing a lumped segment of cable, which were presented in the previous section, can now be implemented using the elements of bond graph representation. One element not mentioned in Chapter 3's introduction to bond graphs was the "field" element. Due to the nature of this modeling, when considering movement in two dimensions in space it is convenient to construct a multiport element for the spring, or "C-field". The C-field will contain expressions for the spring and damping, which were developed in the previous section, to allow the exchange of power port variables velocity (generalized flow) and force (generalized effort) between the previous and subsequent elements in the chain.

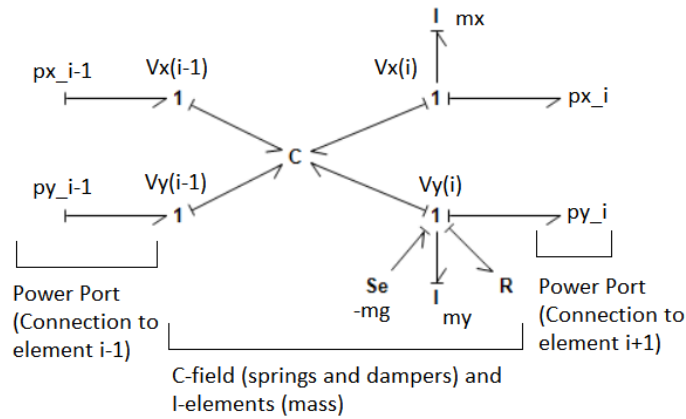


Figure 5.3. Element of Spring/Damper and Mass in Bond Graph (Pinto & Rideout, 2016)

Figure 5.3 shows implementation of an element of the cable in the bond graph representation. Here, 1-junctions correspond to the velocity nodes at the extremity of the spring/damper (C-field) element, such as between the coordinates $x1$, $y1$ and $x2$, $y2$ in Figure 5.2. Attached to the right side of the power bonds connected to the 1-junctions are the mass elements mx and my (I elements) for the x and y coordinates, and the contributions of gravity $-mg$ source of effort (Se element) and viscous damping (R element) for the y coordinate.

The masses (I elements) are therefore attached to the x and y 1-junctions along with the C-field, decomposing Newton's law into the two component directions, x and y. Note the additional R element is not present in the equations above; it was added as a mean to provide additional lateral viscous damping.

Velocities are causal inputs to the C-field, and forces are the causal output. Passing through the C-field, velocity will be integrated, resulting in displacements of the spring/damper. Causality is emphasized by the short strokes at the power bonds arriving at the 1-junctions.

Cable Bond Graph on the Connection Points

Implementation of boundary conditions at both extremities of the cable model is necessary to hold the cable at fixed points, and for the connection between pole and cable models.

The cable is considered to be fixed by pinned connections on the supports at both extremities. To produce the pinned connection, it is necessary to attach a zero-valued generalized source of flow at both of the coordinates x and y . However, if we simply introduce the source of flow to the cable element as presented in the previous section, that would cause a causality conflict in the model because the velocity (flow) is directed by each submodel to the extremity. Since it is convenient to avoid causalities in order to produce explicit ordinary differential equations in the model, modifications were made on the last lumped element of the cable.

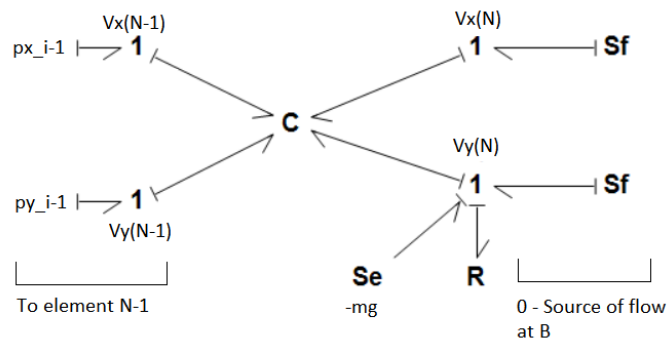


Figure 5.4. Termination Element of Cable (Pinto & Rideout, 2016)

Figure 5.4 presents the termination element of the cable where the mass elements in the x and y directions are removed and the sources of zero flow are added. The mass is then

redistributed through the other elements in the chain and the last element becomes a spring/damper only element.

In the case where the pole model is connected to the cable model, lateral motion (velocity) of the pole is bonded to the horizontal motion (x direction) of the cable, leaving the y direction velocity connected to a zero-flow source, since no motion is expected in that direction.

Excitation sources are added to convenient locations along the cable to emulate hammer hits, or to emulate sudden impulses caused by plucking the cable. The excitation sources are effort sources (S_e) that can be added to the 1-junction elements in the y direction to excite lateral motion. Any number of elements could be used to compose the cable chain, depending on the compromise between the frequency range expected and the computational demand. Here, fifteen segments are used and considered sufficient for the capture of the first natural frequencies.

String Equation

As another resource for verification, the results of the modeling above can be first compared to the equation of continua for a vibrating string presented in Inman (2014). The frequencies of a string subjected to tension T [N] and small sag are:

$$f_n = \frac{n}{2L} \sqrt{\frac{T}{\mu}}, \quad n = 1, 2, \dots \quad (5.12)$$

where μ is the linear density and L is the length of the string.

Proposing a Physical Model for Testing the Cable Model

Cables exist in diverse constructions and are used for different applications. Due to availability, for the physical model a steel cable was used to represent a scaled electric line. The properties of the 7x7 stainless steel stranded cable were: length of 3.6 meters, diameter of 8.35 mm, density of 9537 kg/m^3 , and elastic modulus of 195 GPa. Cable density was estimated by measuring the volume of a single strand and the total weight. Since the exact manufacturer was not known, modulus of elasticity was obtained from the averaged value found in similar cable datasheets.

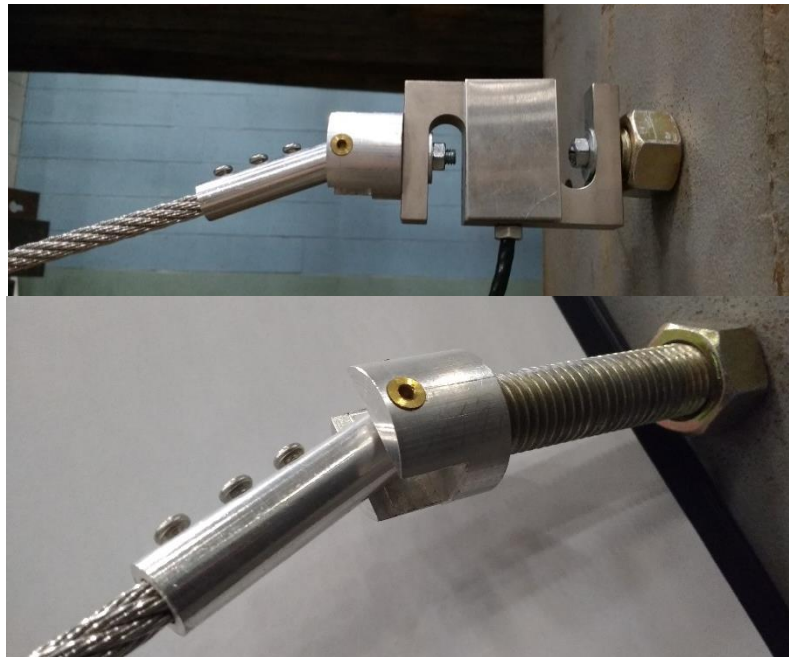


Figure 5.5. Connector with and without Load Cell and Threaded Rod to Hold the Cable

To connect the cable to the other components of the physical model, a set of mechanical parts was designed and produced allowing motion of the cable in the vertical direction.

Figure 5.5 shows the connector and the threaded rod holding the cable on a support at the laboratory. The threaded rod can allow tension adjustments.

Because the stranded cable presented here is different from the simulated model, i.e., multiple wires with some torsional effects and friction, discrepancies are to be expected.

Adding the Third Dimension

The possibility of testing the pole in different directions relative to the electrical lines requires an extension of the developed cable model to the third spatial dimension. This development can be used in the future by researchers continuing this project, and will not be explored through any simulation or development in this work.

Modification of the model to allow for spatial motion, by adding the z direction, requires the addition of some previously presented equations.

Equation 5.6 for the length of the spring/damper element becomes:

$$\delta_e = \sqrt{(x_2 - x_1)^2 + (y_2 - y_1)^2 + (z_2 - z_1)^2} - l_e \quad (5.13)$$

Derivative of Equation 5.13 results in the velocity on the axial direction of the spring/damper.

$$\dot{\delta}_e = \frac{2(x_2 - x_1)(\dot{x}_2 - \dot{x}_1) + 2(y_2 - y_1)(\dot{y}_2 - \dot{y}_1) + 2(z_2 - z_1)(\dot{z}_2 - \dot{z}_1)}{2\sqrt{(x_2 - x_1)^2 + (y_2 - y_1)^2 + (z_2 - z_1)^2}} - \dot{l}_e \quad (5.14)$$

Equations 5.10 and 5.11 become Equations 5.15 and 5.16 and the complements of Equation 5.17.

$$F_x = F \cos(\alpha_e) \quad (5.15)$$

$$F_y = F \sin(\beta_e) \quad (5.16)$$

$$F_z = F \sin(\gamma_e) \quad (5.17)$$

And Equation 5.8 is replaced by angles in all three directions:

$$\alpha_e = \arccos \frac{(x_2 - x_1)}{\delta_e} \quad (5.18)$$

$$\beta_e = \arccos \frac{(y_2 - y_1)}{\delta_e} \quad (5.19)$$

$$\gamma_e = \arccos \frac{(z_2 - z_1)}{\delta_e} \quad (5.20)$$

Similarly, as previously done, these equations can be implemented into a C-field using bond graph formalism. Figure 5.6 presents the bond graph representation of one element showing the power ports correspondent to each orthogonal direction x , y , z .

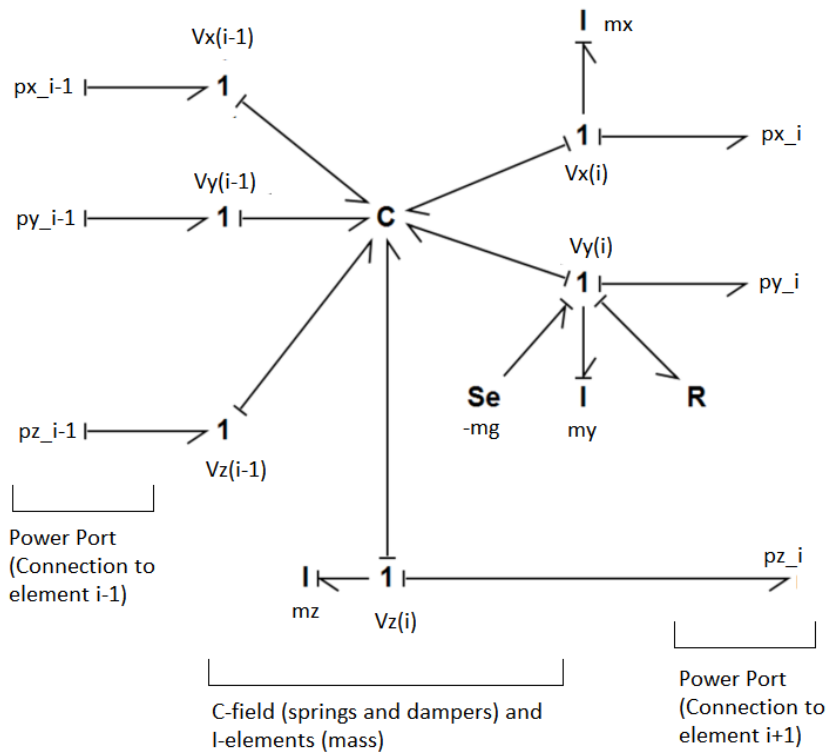


Figure 5.6. Three-Dimensional Element of Cable Implementation in 20sim

Note that mass element I is attached in all directions, with gravity and linear drag damping still attached only in the y direction.

Appending a drag damping element to the z direction as well is straightforward.

Chapter 6 - Proposed Tests for Model Verification

Previous chapters presented the formulation of the sub models for the pole and cable, while in this chapter a set of tests is proposed to obtain experimental data for comparison with the models' results. The pole, reduced to a bar here, is subjected to modal testing and plucking, and the FRF and time series are registered. Similar tests are performed on the cable alone, and on the cable when connected to the bar. These tests can be replicated in simulation. The results are compared in the next chapter, Results and Discussion. Additional tests are proposed as proof of concept for attempts to increase damping along the bar and to verify changes in the total system response spectrum.

Pole and Cable Materials

The properties of the available materials for the pole (copper bar) and cable (49-strand stainless steel) scaled structure were determined using the methods presented in the previous chapters and summarized here in Table 6.1.

Table 6.1. Materials Properties

	<i>Material</i>	<i>Length (m)</i>	<i>Elastic Mod. (GPa)</i>	<i>Density (Kg/m³)</i>	<i>Area (m²)</i>
<i>Pole</i>	Copper bar 31.75 x 6.35 mm	1.15	119	8910	2.01x10 ⁻⁴
<i>Cable</i>	Stainless steel 7x7 wires	3.6	195	9537	2.78x10 ⁻⁵

Modal Testing Procedures

The bar (representing a pole) and cable were subjected to impact modal tests. After proper configuration in ModalVIEW, the hammer was used to produce five separated FRFs which were averaged and saved for posterior frequency and damping extractions according to the methods previously presented.

The bar was clamped at one of its extremities, leaving the free side pointing towards the ceiling of the laboratory (see Figure 6.1a). Then two accelerometers were fixed to the bar, at the tip and at 25 cm from the clamp.

Modal testing was also performed on the cable alone, for several different tensions with very little sag (91.4, 104.5, 140.6, 230.8 N) and one tension with sag (15.5 N in the horizontal direction). Two accelerometers were used in this test, being affixed at 0.3 and 1.8 m from one of the cable's extremities. Hammer hits were applied at 1/4 and 1/5 of the cable span (see Figure 6.1b).

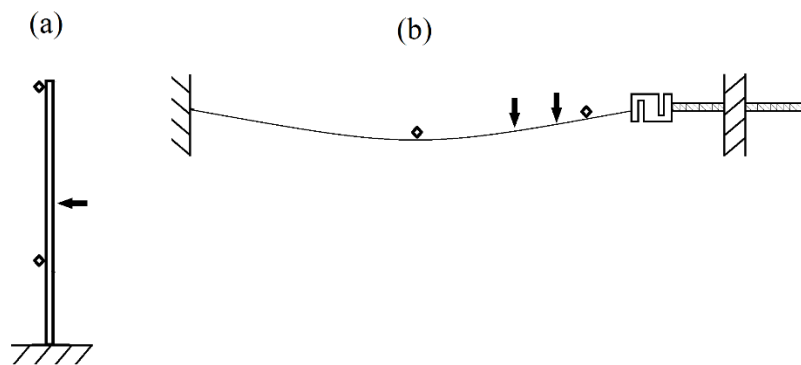


Figure 6.1. Modal Testing over Bar and Cable

In Figure 6.1, the “S” shaped figure on the right side represents a load cell, the black arrows represent hammer hit locations, and the diamond icons indicate accelerometer positions. For tension adjustments, the load cell was attached to a threaded rod. Finally, modal testing was performed on the bar and cable while connected. The left side of the cable presented in Figure 6.1b is then fixed to the tip of the bar in Figure 6.1a. Here, the accelerometers were positioned only on the bar and in the same way as for the bar alone. Figure 6.2 illustrates the connected set-up.

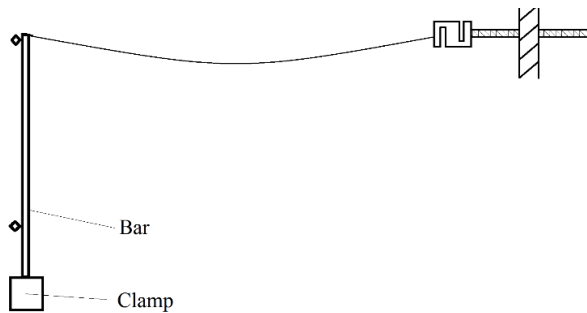


Figure 6.2. Experimental Set-Up for Cable and Pole Model Verification (Pinto & Rideout, 2016)

Time Series Procedures

Time domain tests for the physical model were also proposed for dynamic verification of the bar and cable system. As done previously with the modal testing, time series tests are first performed on the bar alone, then on the cable alone, and then on both connected.

The bar was firmly held to a rigid metallic structure using C-clamps. The other extremity points at the ceiling and was able to vibrate in the horizontal direction. Then the bar was assembled to the string-pulley-mass system (see Figure 6.3a). In Figure 6.3a, the diamond icon at the tip of the bar indicates the position of an accelerometer used for the time series

recordings. Finally, the bar can be excited by one cutting of the string, and the time response was properly recorded for posterior analysis.

The cable test was performed similarly. First, the cable was fixed at its two extremities using the designed connectors presented in Chapter 5. One cable extremity was fixed directly to a rigid structure, leaving the other extremity to be connected to a load cell which was fixed to the other support. Cutting the string will excite the accelerometer positioned at the middle of the cable span (see Figure 6.3b).

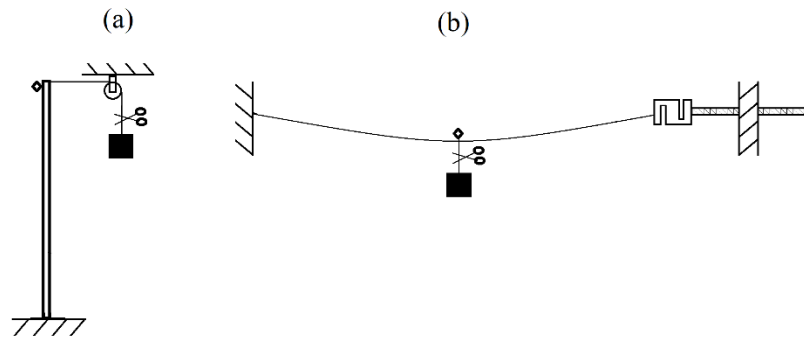


Figure 6.3. Schematic of Time Series Tests

Finally, the test is performed over the bar and cable connected. The right side of the cable is attached to the tip of the bar with the mass held on the cable. In this case, time series is recorded using the accelerometer attached to the bar. The final configuration is similar to Figure 6.3a with cable of Figure 6.3b. The horizontal component of tension for the combined case was recorded as approximately 15 N.

Procedures for Adding Damping to the Bar

To add damping to the bar without causing a significant increase in weight, cardboard panels were fixed to the bar with the aid of double sided tape. Figure 6.4 illustrates the bar with the added panels.

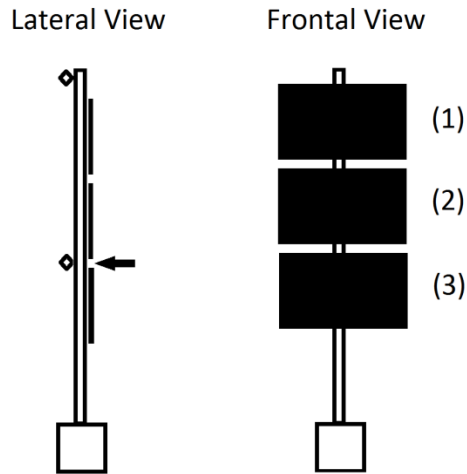


Figure 6.4. Schematics of the Bar Configurations for Additional Damping

In this case, the bar was held as previously, but with a second accelerometer positioned at half-length on the bar, with hits performed in the same place, between the cardboards. To facilitate test arrangements, the cardboards were numbered in combined groups: 0 (no cardboard), 1 (for one cardboard piece), 2-3 (for 2 and 3 cardboard pieces) and 1-2-3 (with all cardboard pieces), Figure 6.4.

Modal testing was performed for the bar alone and using these combinations of cardboard pieces and the same was done for the combined system, pole and cable. However, not all the cases tested will be presented in the Results and Discussion chapter.

Chapter 7 - Model Verification and Added Damping: Results and Discussion

The proposed verification tests discussed in the previous chapter were expected to yield three results for the bar, cable, and system bar / cable configuration: the measured results from the modal testing, the expected results from the theory application of the proposed properties and geometry, and the results from the simulations.

Note that in the case of the bar simulations, the damping obtained from the modal testing of the bar alone is used together with its properties and geometry to produce the model used in this comparison. Equation 4.16 converts the percentage damping to the resistance element added to each mode oscillator in the bond graph model. These resistances are: 1.396, 1.946, 2.072, 13.156, 3.9366 N-s/m.

In addition, the results of the proposed methods for changing the bar damping and its influence on the overall behavior of the system are discussed.

Verifying the Pole Model

Five modal damping ratios associated with their respective frequencies are used in the simulation bond graph diagram presented in Chapter 4. Therefore, the same number of modes are retained from the modal testing performed on the bar. Table 7.1 presents the

results of the tests and simulations, and compares the frequencies obtained from the simulations with the frequencies observed in the tests.

Table 7.1. Pole Frequency Response, Modal Testing and Simulation (Pinto & Rideout, 2016)

<i>Modes</i>	<i>Modal testing</i>		<i>Simulation</i>	
	<i>Frequency Hz</i>	<i>Damping %</i>	<i>Frequency Hz</i>	<i>Frequency Error %</i>
<i>1st</i>	2.660	2.021	2.474	6.9
<i>2nd</i>	17.153	0.437	17.618	2.7
<i>3rd</i>	48.078	0.166	49.322	2.5
<i>4th</i>	94.721	0.535	96.638	2.0
<i>5th</i>	156.319	0.097	159.791	2.2

It is noticeable from the table above that the simulations fairly closely reproduce most of the chosen frequencies of the bar, with errors less than 3%, the first mode being the most different.

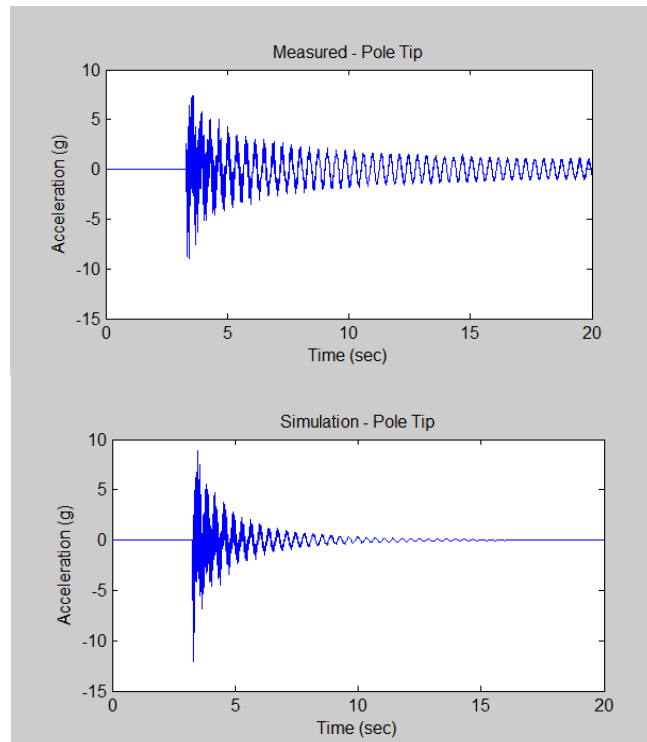


Figure 7.1. Acceleration Time Series for Pole Tip, Measurement and Simulation (Pinto & Rideout, 2016)

Figure 7.1 shows the results of the time series test on the bar using an accelerometer at the tip of the bar. The simulation result is shown in the lower part of the figure.

The measurement result appears to indicate a damping that is lower than that in the simulated model. Despite that, the initial amplitudes are similar. In the measured case, there is a constant oscillation after a long period of time (more than 20 seconds). This effect might be due to gravitational force acting on the distributed mass of the bar that was vertically positioned.

Verifying the Cable Model

Experimental modal analysis is performed on the cable to identify dynamic properties in diverse cable tensions. These results are compared to the theoretical expected values for a vibrating string with the same properties and geometry, and compared also to the cable simulation results. The simulated cable was excited using an effort source pulling the cable to an initial deflected state. The effort source was then set to zero after some time, resulting in free vibration. Results with small sag and higher tension can be seen in Table 7.2.

A comparison of the frequencies obtained using the different methods are consistent with an error of around 10%. However, it is noticeable that in two cases the simulation was not able to capture the first mode. This was due to the difficulty during simulation of inducing excitation in the cable in a way that would allow capture of the first mode. Other attempts, changing the effort source, captured frequencies in the missing interval, between 2.5 and 3.5 Hz, which is consistent to the previous results. This inconsistency might be due to

numerical tolerances in the *20sim* transfer function generator applied to the lumped segment model.

Table 7.2. Cable Frequencies: Theoretical, Modal Test and Simulation. (Pinto & Rideout, 2016)

<i>Tension</i>	<i>Theoretical</i>	<i>Modal Testing</i>		<i>Simulation</i>	
	<i>Frequency</i>	<i>Frequency</i>	<i>Damping</i>	<i>Frequency</i>	<i>Damping</i>
<i>N</i>	<i>Hz</i>	<i>Hz</i>	<i>%</i>	<i>Hz</i>	<i>%</i>
91.4	2.581	2.78	1.751	2.563	0.45
	5.161	5.141	4.766	4.501	0.28
	7.742	7.274	1.411	6.891	0.16
104.5	2.759	-	-	-	-
	5.519	5.991	3.055	5.680	0.22
	8.278	7.543	1.243	9.412	0.15
140.6	3.201	3.254	1.409	-	-
	6.402	6.636	1.568	6.729	0.18
	9.602	10.713	2.713	10.775	0.13
230.8	4.101	5.71	2.691	5.397	0.31
	8.202	8.611	1.217	8.827	0.23
	12.303	13.155	1.573	13.151	0.33

The lumped segment model is not able to match the damping ratios, so it is necessary to attempt to tune it by varying the overall damping applied to the cable, or by varying lateral damping (Resistor added to the 1-Junction in the y direction discussed in Chapter 5).

Test results with sagged cable and low horizontal tension (15.5 N) are:

Table 7.3. Sagged Cable Measurements

<i>Modes</i>	<i>Modal testing</i>	
	<i>Frequency</i>	<i>Damping</i>
	<i>Hz</i>	<i>%</i>
<i>1st</i>	2.487	3.339
<i>2nd</i>	4.133	12.285
<i>3rd</i>	6.659	4.717

Sagged cable tests were performed because sagging is a condition expected of electric cables in the field.

Time series experiments on the cable were performed based on the proposed conditions in the previous chapters. A cable tension of 191 N is used for tests and simulations, and is inside the range of tensions in Table 7.2. Figure 7.2 shows a 20 second time series using an accelerometer positioned at the half span of the cable. Amplitudes are similar. However, the measured response is damped slower than in the simulation, demonstrating the necessity of final tuning of the damping. In addition, it is possible to observe some beat frequencies in the simulated result, perhaps caused by high frequency modes introduced by the lumped segmentation technique.

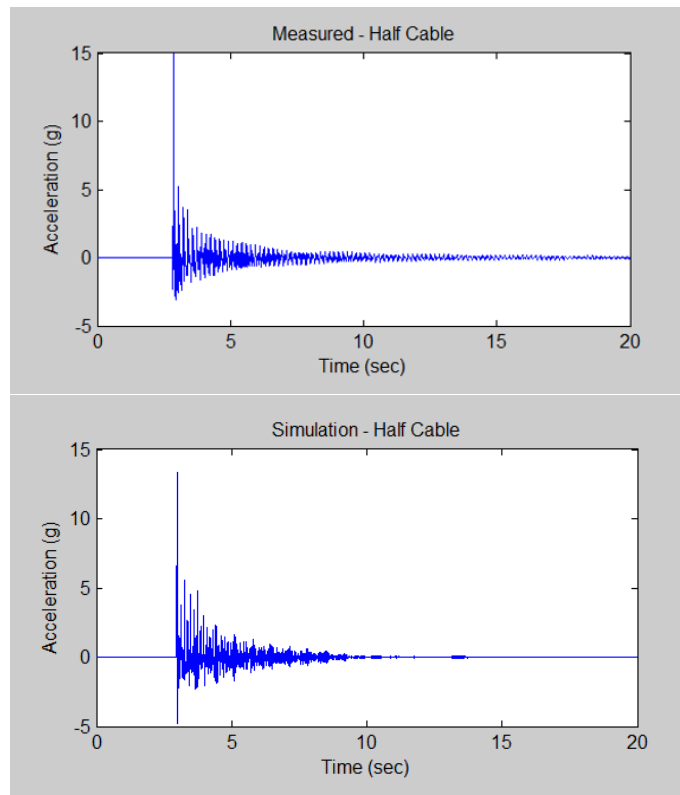


Figure 7.2. Acceleration Time Series of Cable Tests (Pinto & Rideout, 2016)

Cable and Pole Model Verification

Table 7.4 presents the results of modal testing and the simulation of the bar and cable.

Table 7.4. Bar-Cable System Frequency Response, Modal Testing and Simulation (Pinto & Rideout, 2016)

<i>Modes</i>	<i>Modal Testing</i>		<i>Simulation</i>		
	<i>Frequency</i>	<i>Damping</i>	<i>Frequency</i>	<i>Damping</i>	<i>Frequency</i>
	<i>Hz</i>	<i>%</i>	<i>Hz</i>	<i>%</i>	<i>Error %</i>
<i>1st</i>	1.401	4.397	1.504	1.18	7.40
<i>2nd</i>	4.474	2.784	4.709	0.24	5.26
<i>3rd</i>	10.038	3.145	10.047	0.11	0.09
<i>4th</i>	12.677	0.955	13.066	0.46	3.07
<i>5th</i>	40.268	0.428	40.934	0.19	1.65
<i>6th</i>	83.550	0.606	84.877	0.49	1.58

The system ensures low errors in frequency between the simulation and the bar modal testing. However, modal testing performed according to the method suggested in Chapter 3 was not able to detect all of the frequencies obtained in the simulation. System simulation produced frequencies that are not shown in Table 7.4, but they do seem to be relatable to the cable frequencies in Table 7.3, being: 2.37, 4.70, and 6.79 Hz. The lumped segmentation method used for the cable caused a discrepancy due to the appearance of higher frequencies. However, for the range of low frequencies investigated, it seems to be reasonable to use this model.

Time series tests were also performed on the system bar-cable, and acceleration at the bar tip was recorded (see Figure 7.3).

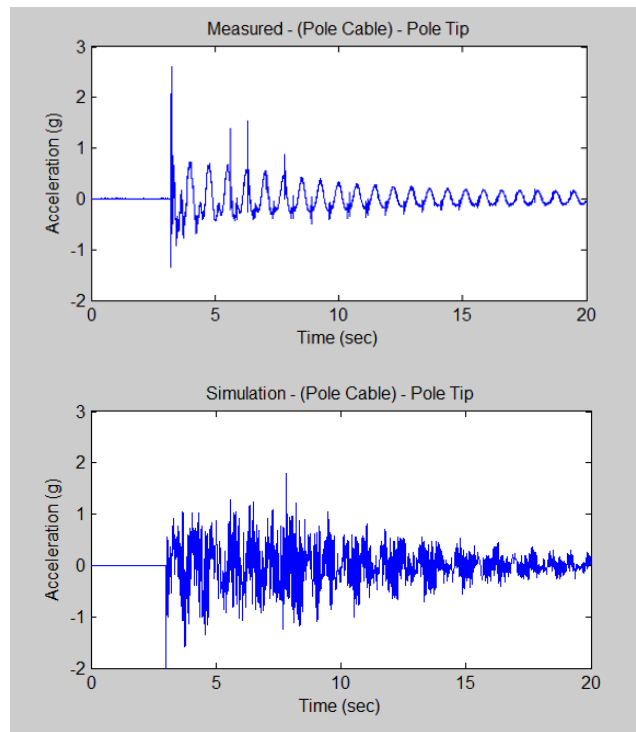


Figure 7.3. Acceleration Time Series for the Pole and Cable Connected. (Pinto & Rideout, 2016)

The cable model had the damping ratio tuned to match the time series decay seen in Figure 7.2, and the high frequencies continue to appear in the combined system as shown in Figure 7.3. The simulations therefore contained frequencies not present in the tests.

The stabilization chart used to obtain the damping and frequencies shown in Table 7.4 is presented in Figure 7.4.

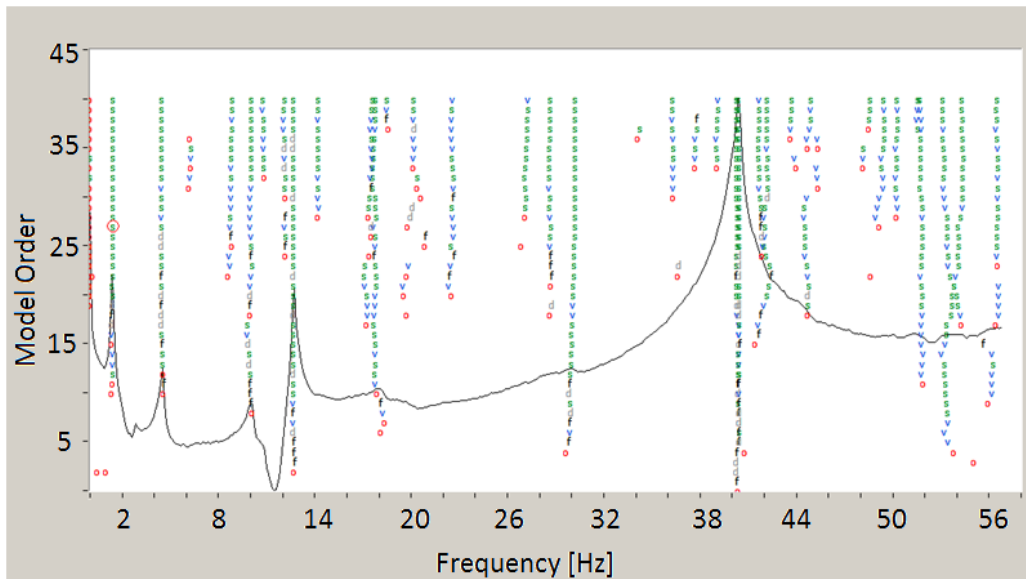


Figure 7.4. Experimental Stabilization Chart of the Pole and Cable (Cable Tension 15N) (Pinto & Rideout, 2016)

A comparison of the first three frequencies in Table 7.1 (from the “pole”) with the FRF presented in Figure 7.4 indicates that the addition of the cable shifted the frequencies, lowering them considerably.

Previously, it was presented that the first frequency of the cable was designed to correspond to the first frequency of the bar. This caused the reduction in the frequency in the combined system.

Even though the model seems to match closely, the test results and the verification suggests a good approximation, it seems that there is a significant difference between measurements obtained from the bar alone and measurements obtained from the combined system. However, there is still room for more exploration. In the proposed test, the cable that was used was significantly thicker and heavier than the bar, obviously resulting in a greater

interaction with the bar. In addition, the excitation direction of the bar was in the same direction as that of the cable, amplifying its influence even more.

Additional Damping and System Behaviour

Proceeding according to the method presented in Chapter 6, four tests were chosen to be presented: the bar without any cardboard (condition 0), the bar with the cardboard panels (combination 2-3), the bar and the cable without cardboard, and the bar and cable with cardboards 2-3. Figure 7.5 shows the FRFs from the new test with the bar, with and without additional damping and now including a wider range of frequencies, from 0 to 512 Hz.

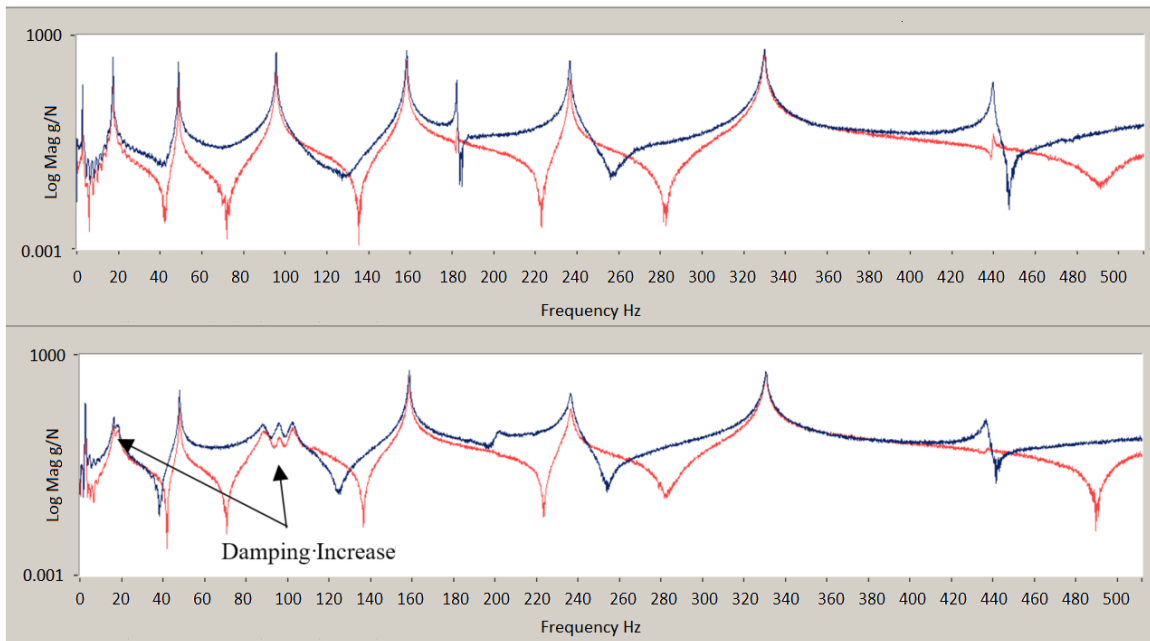


Figure 7.5. Transfer Function of the Bar, without Damping (Top) and with Damping 2-3 (Bottom), Blue is the Accelerometer at the Tip, Red is the Accelerometer at Mid-way

The FRF of the bar without additional damping is clear and allows the recovery of at least 8 clear modes. With the additional damping, the second mode in low frequency seems to

be attenuated, with the single peak of the 4th mode at the top, changing to three smaller peaks in the FRF at the bottom. The chart in Figure 7.6 was generated by extracting the frequencies and damping ratios of both scenarios. The observations for the FRFs are then confirmed, because in the low range (below 150 Hz) it is possible to observe some change in damping, but after that there is not much effect.

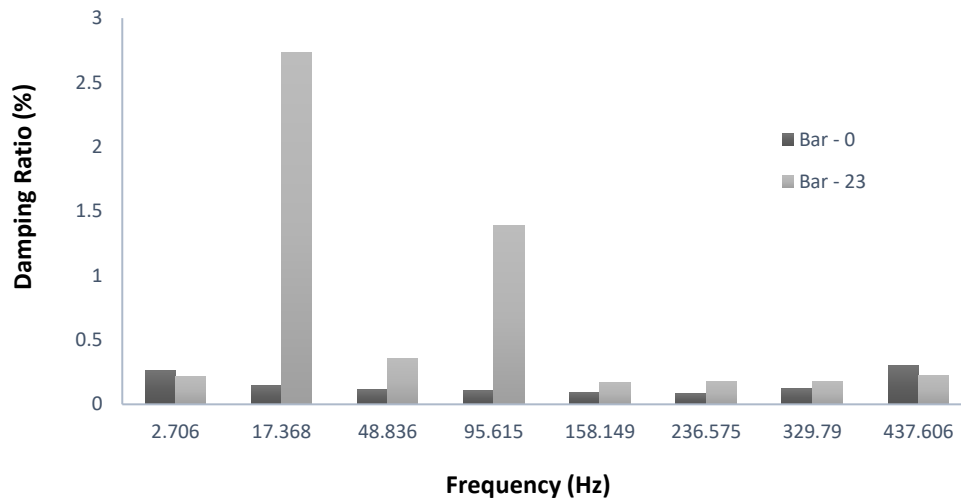


Figure 7.6. Variations in Bar Damping – Before and After Damping Increase

Impact test was performed on the bar with additional damping while it was connected to the cable. This test was intended to verify whether bar damping could be detected even when the bar is connected to the cable. The transfer function of this measurement is presented in Figure 7.7. The overall aspect of the FRFs is the same, except that the bottom image seems to have more noise. By comparing the previous measurements of the bar alone with these new ones, it is noticeable that the frequencies are considerably lowered.

The frequencies and damping ratios of the system without damping and with additional damping are presented in Table 7.5. Six peaks were chosen. When comparing both

scenarios (with and without damping) the frequency slightly decreases and the damping ratios showed increased values, except in the 4th mode.

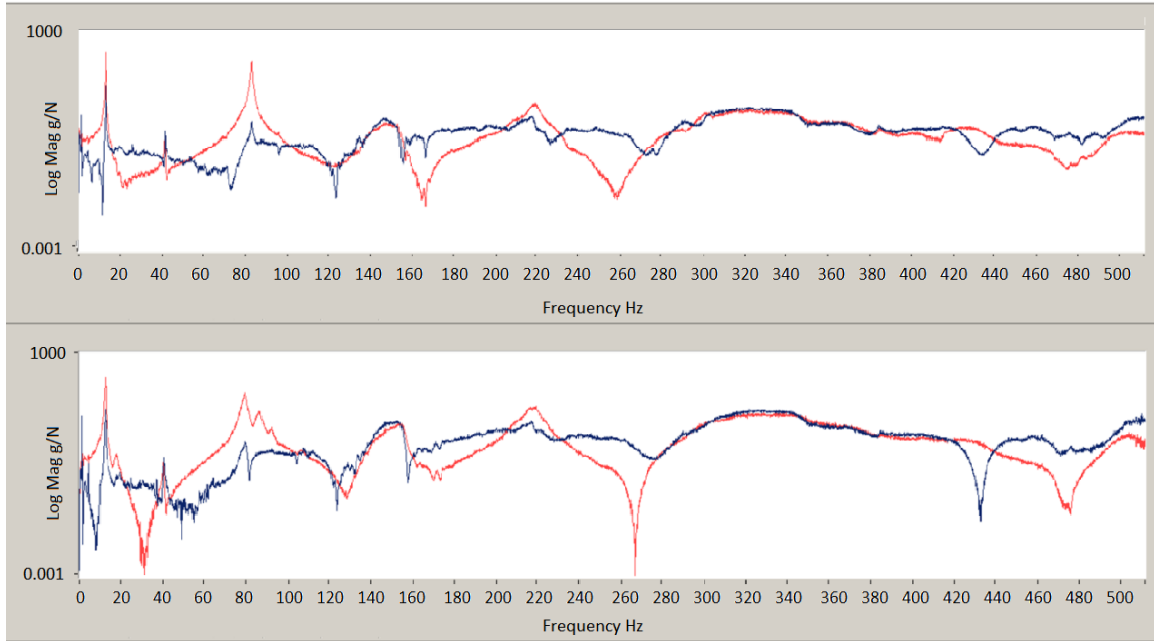


Figure 7.7. Transfer Function of the Bar and Cable, without Damping (top) and with Damping 2-3 (bottom), Blue is the Accelerometer at the Tip, Red is the Accelerometer at Mid-way

Table 7.5. Results of Modal Testing on Bar and Cable with/without Additional Damping.

	<i>Bar and Cable without Additional Damping</i>		<i>Bar and Cable with Additional Damping</i>	
	<i>Frequency</i>	<i>Damping</i>	<i>Frequency</i>	<i>Damping</i>
<i>Modes</i>	<i>Hz</i>	<i>%</i>	<i>Hz</i>	<i>%</i>
1	12.872	0.315	12.536	0.683
2	40.988	0.212	40.214	0.376
3	83.032	0.629	79.673	1.733
4	144.87	2.774	154.92	1.202
5	219.59	0.789	217.438	2.07
6	317.711	5.006	320.5	6.242

As per Table 7.5, the frequencies of the system do not change much with additional damping. Showing that, though we can't identify the exact frequencies of the pole (all

frequencies are reduced when comparing with the frequencies of the pole alone), we still able to verify the changes in damping ratio between correspondent frequencies. This points to the necessity of having a database of the system (pole and cables) over the life of the pole, i.e. collect measurements of the system along the lifespan of the network. Since the cable and other equipment will present slightly changes in damping, the changes in the system damping can be attributed to the pole decay.

Figure 7.8 presents the changes in damping of the bar and cable before and after the increase in damping ratio. The damping increases much less than when the bar is alone (see Figure 7.6), it suggests that it becomes more difficult to extract information related to the damping ratios of bar when it is interacting with other systems.

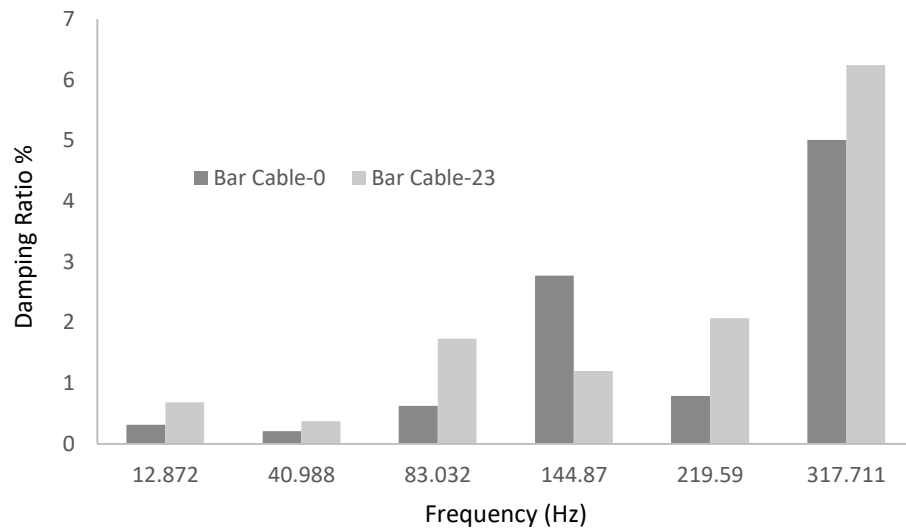


Figure 7.8. Variations in Bar/Cable Damping – Before and After Damping Increase

Chapter 8 - Conclusions and Future Work

This work was a preliminary study of the dynamic response produced by attaching electrical cables to wooden poles subjected to non-destructive tests. Three main objectives were proposed: to develop a simulated model of a pole and cable using the bond graph formalism, to design a reduced scale system containing a pole and a cable to be used for verification of the models, and to use the reduced system to obtain insight into how a cable dynamically interacts with a pole, aiming to isolate these effects in the future.

Modal expansion through separation of variables was used to model the pole, and the lumped segmentation technique was used for the cable model. An experimental setup composed of a copper bar and a steel cable was assembled and used to verify the model. Time series testing and modal testing were performed on the physical model, and the dynamic results were compared to the simulated ones. Frequencies in both models presented overall good agreement for the low frequency range studied. The Euler-Bernoulli beam and modal expansion were verified to be an excellent model for metallic beams undergoing small deflection. The lumped-segment cable model, with 15 elements, could not map the damping ratio appropriately, and time responses also presented some discrepancies. These effects were expected, due to the difficulty of tuning the cable damping and to the spurious frequencies added to the system, which were inherent to the chosen modeling. The associated model, pole and cable permitted observation of the effects of the cable on the frequencies associated with the pole. However, future improvements are necessary to obtain better results.

The tests on the reduced physical model, modified with the addition of drag damping to the bar, lead to two main conclusions: First, it is possible to add damping by using the proposed method, with greatest effects being perceived in the lower modes. Second, the influence of the cable on the bar is immense for the reduced model, partially because the weight of the cable was applied to only one side of the bar (there being no other pole to share the weight), and the direction of the hits favoured excitation of the cable. These conclusions point to the necessity of future improvements in the reduced test apparatus.

Future Work

The pole model developed using modal expansion can map frequencies with very small error for the constant properties of a solid regular section metal bar. However, this is the case for this reduced metal model, not for a real wooden pole which does not have constant properties, has defects, and is tapered from the bottom to the top. The tapering factor was already addressed in a model presented by Rideout & Whelan (2014), and can be used in future work in association with cable models.

The cable model presented can reproduce the frequencies measured. However, it also created many spurious frequencies due to the nature of lumped segmentation. If other attachments common to electric power transmission networks (i.e. more cables, isolators, guy cables, etc.) are included in the future, errors caused by extra numerical frequencies might be amplified in the overall result. For this reason, an improvement in the model would require a process of optimization in the number of segments, or a complete change

in the lumped segment, using rigid bodies, rotational inertia, bending stiffness and other damping mechanisms.

Another approach for modeling the cable could be to explore the separation of variables done for strings in Inman (2014). Similar to what was done for pole modeling, it could be done for the cable, to permit tuning damping on the model according to measured values.

In the physical model, the cable used was proportionally heavier in comparison to the pole weight, and this highly influenced the total response of the system. Future work on a physical model should use a cable with reduced diameter as well. In a real situation, the cable diameter is only a small fraction of the pole diameter, and usually the pole stands between other poles, balancing the effort.

In this study, the experimental setup was not scaled down from the real pole and cable using similitude laws for dynamics. However, future work should consider scaling new models using similitude given the considerable research that has been developed in this area. The work of Balawi et al. (2015), for example, developed similitude laws for beams and plates performing experiments and testing the results against finite element analysis finding good results. Another example comes from Wilson (2014), whom also employed scaling laws for dynamics for the study of flawed utility poles by deriving the equations of motion to use in reduced scaled laboratory models.

In testing a real pole in the field, it is possible to impact the pole in at least two directions: perpendicularly, or parallel to the electrical lines. The models presented so far allow the cable to move only in the vertical direction (y) and the hitting effort is parallel to the line. Therefore, new implementations are necessary by extending the cable model to the third

dimension, which necessarily implies a modification of the test setup. Currently, a 3D lumped model based on the presented theory has been implemented, but not yet verified.

The simulations were performed using a commercial software to assemble the bond graph formalism and to solve the differential equations created according to the formulations presented. However, as most of the software packages, not all methods used in solving the equations can be seen in details and other tools could be used for modeling and verification in future work.

In conclusion, other attachments (cross bars, isolators, etc.) still need to be modeled and more cables and poles need to be included to extend this work and obtain a deeper understanding of the influence of such systems in each of the pole's responses. Besides, the increase in complexity of these models might require the use of other simulation tools. Simulations using the method of separation of variables and lumped segmentation could be also compared to the results of a finite element analysis of the pole and cable. Extensive material has been developed to allow the modeling of dynamic parameters, such as modal frequency and damping, using FEA formulation.

Improvements on the simulated models need to be done based on field tests and cumulative data, in order to achieve a model that better represents the reality of wooden poles interactions. Thus, the research group that is continuing this work predicts the future necessity of implementing specific software/hardware for the dynamic extraction of wooden pole properties, including those of developed models.

Bibliography

Balawi, Shahid, & Mulla. (2015). Similitude and scaling laws - Static and dynamic behaviour beams and plates. *Procedia Engineering*, 114, 330-337.

Barbieri, N., Júnior, O. H., & Barbieri, R. (2004). Dynamical analysis of transmission line cables. Part 1—linear theory. *Mechanical Systems and Signal Processing*, 18(3), 659-669.

Billah, K., & Scanlan, R. (1991). Resonance, tacoma narrows bridge failure, and undergraduate physics textbooks. *American Journal of Physics*, 59(2), 118.

Bodig, J. & Phillips, G. E. (1984). Mechanical proprieties of wood utility poles. *Proc. Annual Meeting of The American Wood-Preservers' Association*. 128-138.

Datla, S. V., & Pandey, M. D. (2006). Estimation of life expectancy of wood poles in electrical distribution networks. *Structural Safety*, 28(3), 304-319.

Dillon, P., PEng. (2009). 2009 Wood pole line management - A report to the board of commissioners of public utilities. Retrieved October 18, 2016, from <http://www.pub.nf.ca/applications/NLH2009Capital/files/application/NLH2009Application-VolumeII-Report4.pdf>

Downer, L. M. (2010). *Detecting damage in beams and structures through modal analysis*. M.Eng. Thesis, Faculty of Engineering and Applied Science, Memorial University of Newfoundland, St. John's, Canada.

Ewins, D. J. (2000). *Modal testing: Theory, practice, and application* (2nd ed.). Baldock, Hertfordshire, England; Philadelphia, PA: Baldock, Hertfordshire, England; Philadelphia, PA: Research Studies Press.

Figliola R. S., Beastley, D. E. (2011). *Theory and design for mechanical measurements*. (5th ed.) USA: John Wiley & Sons, Inc.

Forest Products Laboratory. (1999) *Wood handbook: Wood as an engineering material*. General Technical Report FPL-GTR-113. Madison, WI: U.S. Department of Agriculture, Forest Service, Forest Products Laboratory. 463 p. Retrieved (2, June, 2016) from Forest Products Laboratory <http://www.fpl.fs.fed.us/documnts/fplgtr/fplgtr113/fplgtr113.htm>

Hiller, S. (2016) Hydro to invest \$271.4 million in capital projects in 2017 to strengthen aging grid. Retrieved (8, August, 2016) from Newfoundland Hydro a Nalcor Energy Company: <http://www.nlhydro.com/hydro-invest-271-4-million-capital-projects-2017-strengthen-aging-grid/>

Inman, D. J. (2014). *Engineering vibration*. (4th ed.). Boston, USA: Pearson.

Karnopp, D. C., Margolis, D. L., & Rosenberg, R. C. (2012). *System dynamics: Modeling, simulation, and control of mechatronic systems*. Hoboken, NJ, USA: Hoboken, NJ, USA: John Wiley & Sons, Inc.

ModalVIEW (2012), ABSignal.com.

Morrell, J. J. (2016). Technical Bulletin – Estimated service life of wood poles. *North American Wood Pole Council, No.16-U-101*.

Pinto, P. F. & Rideout, G. (2016). Development and validation of an *in-situ* utility pole model for vibration-based non-destructive testing. *Proc. Int. Mechanical Engineering Congress & Exposition. (IMECE'2016)*, November 11-17, Phoenix, USA.

Qiu, Y., & Maji, A. (2011). Experimental study of cable vibration damping. *Dynamic Behaviour of Materials, Vol. 1*. Conference Proceedings of the Society for Experimental Mechanics Series 99.

Rideout, G. & Whelan, O. (2014). Modeling of tapered cantilever beams for simulation of utility pole vibration. *Proc. Int. Cong. On Bond Graph Modeling and Simulation. (ICBGM'2014)*, July 6-10, Monterey, CA.

Ross, R. J. (1991). In Pellerin R. F., Forest Products Laboratory (US)(Eds.), *Nondestructive testing for assessing wood members in structures: A review* Madison, WI: U.S. Dept. of Agriculture, Forest Service, Forest Products Laboratory.

Scan Pole (2016) Benefits of wooden poles. Retrieved (10, September, 2016) from Scan Pole: <http://www.scanpole.com/benefits-of-wooden-poles/>.

Skjong, S., & Pedersen, E. (2016). Model- based control designs for offshore hydraulic winch systems. *Ocean Engineering*, 121, 224-238.

Spak, K., Agnes, G., & Inman, D. (2014). Parameters for modeling stranded cables as structural beams. *Experimental Mechanics; Exp.Mech.*, 54(9).

Starossek, U. (1994). Cable dynamics - A review. *Structural Engineering International*, 4(3), 171-176.

Tallavo, F., Cascante, G., & Pandey, M. D. (2012). A novel methodology for condition assessment of wood poles using ultrasonic testing. *NDT and E International*, 52, 149-156.

Wilson, J. (2014). Similitude laws and small-scale model experiments characterizing dynamic failures of flawed utility poles. *Journal of Mechanical Design*, 136(9), 091401.

Wood Pole (2016) From forest to decades of service. Retrieved (5, August, 2016) from <http://woodpoles.org/WhyWoodPoles/HowPolesAreMade.aspx>.

20Sim 4.6 (2015) Controllab Products b.v., Enschede, Netherlands.

Appendix A – Data Sheet of the Impact Hammer

Page 1 of 2 in the original document. B&K ©. Full document at:

<https://www.bksv.com/en/products/transducers/vibration/Vibration-transducers/impact-hammers/8206>

Impact Hammers — Types 8206, 8206-001, 8206-002 and 8206-003

USES

- Impact-force measurements on small to medium structures
- Measurement of frequency response functions using impact excitation techniques
- As part of a dynamic structural testing system for modal analysis and the prediction of structural response

FEATURES

- Four types with sensitivity from 1 to 22 mV/N
- Ergonomic handle
- Negligible changes to dynamic properties of test structure
- Three replaceable tips
- Acceleration compensated

Description

This series of Impact Hammers has been designed to excite and measure impact forces on small to medium structures such as engine blocks, car frames and automotive components. An accelerometer (or laser velocity transducer) is used to measure the response of the structure. By using a multichannel FFT analyzer, such as the PULSE™ system, the frequency response function and mode shapes of the test structure can then be derived. Contrary to using an electrodynamic exciter, an impact hammer does not apply additional mass loading to the test object and it provides a very portable solution for excitation.

Characteristics

The Type 8206 series feature built-in electronics and the output sensitivity is expressed in terms of voltage per unit force (mV/N or mV/lbf). The hammers also have built-in acceleration compensation that removes unwanted noise from the resonance of the hammer from the output signal. This results in a clean, smooth output signal representing the excitation in both amplitude and phase.



The impact hammer is supplied with three interchangeable impact tips of aluminium, plastic and rubber. The choice of impact tip determines the impulse shape (amplitude and duration) and the bandwidth of the excitation.

For increased head mass, a 40 gram head extender is available.

The handle has been ergonomically designed for optimal control of impact, thus reducing the risk of “double hits”.

Calibration

The transducer is supplied with an individual calibration of the sensitivity.

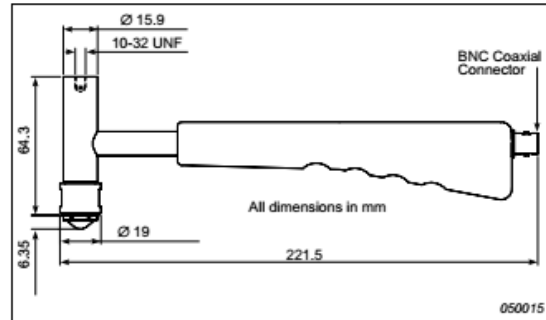
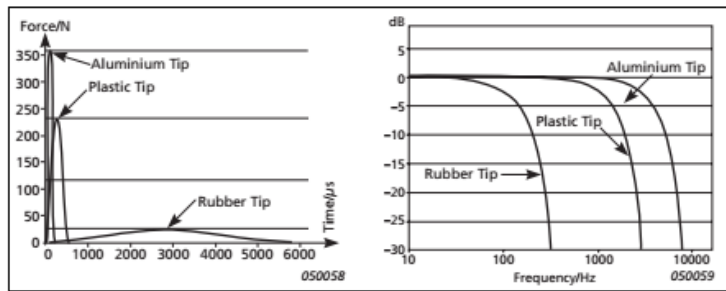


Fig. 1
Impulse shapes for the hammer tips as a function of time showing the pulse decay and peak value (left); Force spectrum of an impact on an aluminium plate (right)



Specifications – Impact Hammers Types 8206, 8206-001, 8206-002 and 8206-003

	Units	8206	8206-001	8206-002	8206-003
Dynamic Characteristics					
Voltage Sensitivity (typical)	mV/N (mV/lbf)	22.7 (100)	11.4 (50)	2.27 (10)	1.14 (5)
Full Scale Force Range Compression	N (lbf)	220 (50)	445 (100)	2200 (500)	4448 (1000)
Linear Error at Full Scale	% full scale	<±1			
Electrical Characteristics					
Full Scale Output Voltage	V	+5			
DC Output Bias Voltage	V	10 ±1			
Output Impedance	Ω	<100			
Power Supply	mA	2 to 20			
Voltage Range	V DC	+18 to +30			
Environmental Characteristics					
Temperature Range	°C (°F)	-73 to +60 (-100 to +140)			
Max. Force Compression	N (lbf)	4448 (1000)			8896 (2000)
Physical Characteristics					
Dimensions		See outline drawing			
Overall Length	mm (in.)	221.5 (8.72)			
Effective Seismic Mass	gram (oz.)	100 (3.53)			
Sensor Housing Material		Stainless steel (17-4 PH)			
Handle Material		Fibreglass			
Connector		BNC			

All values are typical at 25°C (77°F) unless measurement uncertainty is specified

COMPLIANCE WITH STANDARDS



Compliance with EMC Directive and Low Voltage Directive of the EU



Compliance with the EMC requirements of Australia and New Zealand

Ordering Information

Type 8206, 8206-001, 8206-002 and 8206-003 include:

- Impact tip of aluminium
- Impact tip of plastic (Delrin)
- Impact tip of rubber (Polyurethane)
- Carrying box
- Calibration chart
- Head extender (40 grams)
- PVC Insulated Cable, 70°C, 10-32 UNF to BNC Connector, 5 m (16.4 ft)

• Plug Adaptor, BNC to 10-32 UNF

OPTIONAL ACCESSORIES*

- AO 0531: 70°C, Insulated single screen flexible cable, 10-32 UNF to BNC, 5 m (16.4 ft)
- JP 0145: Plug adaptor, BNC/10-32 UNF
- AO 0406: Low-noise, double-screened cable, 10-32 UNF to BNC, 200°C, 5 m (16.4 ft)

- DB 3996: Head extender (40 grams) for Impact Hammer Type 8206
- UA 2059: Set of three impact tips for Type 8206 series impact hammers
- ZZ 0245: In-line TEDS Adaptor, 10-32 UNF to 10-32 UNF

*Additional accessories and cables are available (see www.bksv.com)

Brüel & Kjær reserves the right to change specifications and accessories without notice

HEADQUARTERS: DK-2850 Nærum · Denmark · Telephone: +45 4580 0500 · Fax: +45 4580 1405
www.bksv.com · info@bksv.com

Australia (+61) 2 9889-8888 · Austria (+43) 1 86574 00 · Brazil (+55) 11 5188-8166 · Canada (+1) 514 695-8225
China (+86) 10 680 29906 · Czech Republic (+420) 2 6702 1100 · Finland (+358) 9-521 300 · France (+33) 1 69 90 71 00
Germany (+49) 421 17 87 0 · Hong Kong (+852) 2548 7486 · Hungary (+36) 1 215 63 05 · Ireland (+353) 1 807 4083
Italy (+39) 0257 88061 · Japan (+81) 3 5715 1612 · Korea (+82) 2 3473 0605 · Netherlands (+31) 318 55 9290
Norway (+47) 66 77 11 55 · Poland (+48) 22 816 75 56 · Portugal (+351) 21 47 11 4 53 · Singapore (+65) 377 4512
Slovak Republic (+421) 25 443 0701 · Spain (+34) 91 659 0820 · Sweden (+46) 8 449 8600
Switzerland (+41) 44 880 7035 · Taiwan (+886) 2 2502 7255 · United Kingdom (+44) 14 38 739 000
USA (+1) 800 332 2040 · Local representatives and service organisations worldwide



Appendix B – Data Sheet of the Accelerometer

Page 1 of 12 in the original document. B&K ©. Full document at:

<https://www.bksv.com/~media/literature/Product%20Data/bp1841.ashx>

Miniature DeltaTron Accelerometers — Types 4507 and 4508 Miniature DeltaTron TEDS Accelerometers — Types 4507 B and 4508 B Miniature Charge Accelerometers — Types 4507 C and 4508 C

Miniature DeltaTron® Accelerometers Types 4507 and 4508 consist of a ThetaShear® accelerometer and a DeltaTron preamplifier in a lightweight titanium housing with integrated 10–32 UNF connectors. Types 4507 C and 4508 C are similar to the DeltaTron accelerometers but come without the preamplifier.



USES AND FEATURES

USES

- Modal measurements for automotive body and power-train applications
- Multichannel modal analysis measurements
- Structural analysis measurements

FEATURES

- Robust titanium housing with integrated titanium connector
- Easily fitted to different test objects using a selection of mounting clips
- Low-weight ThetaShear design giving high sensitivity/weight ratio and very low sensitivity to environmental factors
- Triaxial mounting facility

DeltaTron Accelerometers

- Connect directly to DeltaTron power supply (ICP® compatible). The DeltaTron principle allows the use of inexpensive cables. Low output impedance so that long cables can be used
- Built-in, low-noise preamplifiers with ASICs give more than 100 dB dynamic range
- Choice of sensitivities from 10 mV/g to 1 V/g
- ID (TEDS) "Smart Transducer Interface" IEEE – P1451.4 (Types 4507 B and 4508 B)

Charge Accelerometers (4507 C and 4508 C)

- Sensitivity 5 pC/g
- Operating temperature up to 250°C (482°F)

Compliance with Standards

 	CE-mark indicates compliance with: EMC Directive and Low Voltage Directive. C-Tick mark indicates compliance with the EMC requirements of Australia and New Zealand
Safety	EN 61010-1 and IEC 61010-1: Safety requirements for electrical equipment for measurement, control and laboratory use. UL 3111-1: Standard for Safety – Electrical measuring and test equipment
EMC Emission	EN/IEC 61000-6-3: Generic emission standard for residential, commercial and light industrial environments. EN/IEC 61000-6-4: Generic emission standard for industrial environments. CISPR 22: Radio disturbance characteristics of information technology equipment. Class B Limits. FCC Rules, Part 15: Complies with the limits for a Class B digital device.
EMC Immunity	EN 50082-1: Generic immunity standard. Part 1: Residential, commercial and light industry. EN 50082-2: Generic immunity standard. Part 2: Industrial environment. Note 1: The above is guaranteed using Cable AO 1382 only. Note 2: Sensitivity to RF (in accordance with EN 50082-2) 4507, 4507 B, 4507 B 003, 4507 B 004, 4508, 4508 B and 4508 B 003: <60 μV 4507 001, 4507 B 001, 4508 001 and 4508 B 001: <10 μV 4507 002, 4507 B 002, 4507 B 005, 4507 B 006, 4508 002, 4508 B 002 and 4508 B 004: <100 μV
Temperature	IEC 68-2-1 & IEC 68-2-2: Environmental Testing. Cold and Dry Heat. Operating Temperature: 4507, 4507 001, 4507 B, 4507 B 001, 4507 B 003, 4507 B 004, 4508, 4508 001, 4508 B, 4508 B 001 and 4508 B 003: -54° to +121°C (-65° to +250°F) 4507 002, 4507 B 002, 4507 B 005, 4507 B 006, 4508 002, 4508 B 002 and 4508 B 004: -54° to +100°C (-65° to +212°F) 4507 C and 4508 C: -74° to +250°C (-101° to +482°F)

Specifications – Miniature DeltaTron Accelerometers Types 4507

	Sensitivity	Sensitivity Tolerance	Measuring Range	Frequency Range, 10%	Phase Response, ± 5°	Built-in ID (TEDS)	Output Impedance	Bias Voltage	Start-up Time (±10% of final bias)	Inherent Noise (broadband)/ Equivalent Vibration Level	Temperature Coefficient of Sensitivity	Sensing Element	Sealing	Humidity	Mounting Slots (pairs)	
Units	mV/ms ⁻²	%	ms ⁻²	Hz	Hz		Ω	V	s	μV	μg	%/°C		%		
4507	10	±5	700	0.3-6k	2-5k	No	<2	12±1	5	<35	<350	0.09	PZ23	Welded	90	1
4507-001	1	±5	7000	0.1-6k	0.5-5k	No	<2	12±1	50	<8	<800	0.09	PZ23	Welded	90	1
4507-002	100	±10	70	0.4-6k	2-5k	No	<2	12±2	5	<150	<150	0.18	PZ27	Hermetic	100	1
4507 B	10	±5	700	0.3-6k	2-5k	Yes	<30	13±1	5	<35	<350	0.09	PZ23	Welded	90	1
4507 B 001	1	±5	7000	0.1-6k	0.5-5k	Yes	<30	13±1	50	<8	<800	0.09	PZ23	Welded	90	1
4507 B 002	100	±10	70	0.4-6k	2-5k	Yes	<30	13±2	5	<150	<150	0.18	PZ27	Hermetic	100	1
4507 B 003	10	±5	700	0.3-6k	2-5k	Yes	<30	13±1	5	<35	<350	0.09	PZ23	Welded	90	None
4507 B 004	10	±5	700	0.3-6k	2-5k	Yes	<30	13±1	5	<35	<350	0.09	PZ23	Welded	90	3
4507 B 005	100	±10	70	0.4-6k	2-5k	Yes	<30	13±2	5	<150	<150	0.18	PZ27	Hermetic	100	3
4507 B 006	50	±5	140	0.2-6k	1-5k	Yes	<30	13±2	10	<80	<160	0.18	PZ27	Hermetic	100	3

Common Specifications 4507 and 4508 (DeltaTron only)

DYNAMIC

Mounted Resonance Frequency:

4507: 18 kHz

4508: 25 kHz

Transverse Sensitivity: <5% of sensitivity

ELECTRICAL

Constant Current Supply: 2 to 20 mA

Supply Voltage (unloaded):

+24 to +30 VDC (for full specification range)

Min. +18 VDC (reduced measuring range)

Polarity: Positive (for an acceleration in the direction of the engraved arrows)

ENVIRONMENTAL

Max. Non-destructive Shock (\pm Peak): 50 kms^{-2} ; 5000 g

Temp. Transient Sensitivity (3 Hz lower limiting frequency):

4507: $0.2 \text{ ms}^{-2}/^{\circ}\text{C}$

4508: $0.3 \text{ ms}^{-2}/^{\circ}\text{C}$

Base Strain Sensitivity (mounted on adhesive tape 0.09 mm thick): $0.005 \text{ ms}^{-2}/\mu\epsilon$

Magnetic Sensitivity: $3 \text{ ms}^{-2}/\Gamma$

Temperature Range:

4507, 4507 001, 4507 B, 4507 B 001, 4507 B 003, 4507 B 004, 4508, 4508 001, 4508 B, 4508 B 001 and 4508 B 003:

-54° to +121°C (-65° to +250°F)

4507 002, 4507 B 002, 4507 B 005, 4507 B 006, 4508 002, 4508 B 002 and 4508 B 004:

-54° to +100°C (-65° to +212°F)

PHYSICAL

Case Material: Titanium

Sensing Element: Piezoelectric

Design Configuration: ThetaShear

Connector: 10-32 UNF coaxial

Dimensions (H×W×L): 10×10×10 mm (0.4"), excl. connector

Weight: 4.8 gram (0.17 oz.)

Note: All values are typical at 25°C (77°F), unless measurement uncertainty is specified. All uncertainty values are specified at 2σ (i.e., expanded uncertainty using a coverage factor of 2)

Appendix C – Data Sheet of the DAQ

Page 1 of 4 in the original document. National Instruments ©. Full document at:

<http://sine.ni.com/nips/cds/view/p/lang/en/nid/206676>

NI USB-4431 **NEW!**

- One 24-bit analog output
- Four 24-bit simultaneous analog inputs
- ± 3.5 V output range
- ± 10 V input range
- 100 dB dynamic range
- Antialiasing filters
- TEDS read/write
- Software-selectable AC/DC coupling (0.1 Hz HPF)

Recommended Software

- Sound and Vibration Measurement Suite
- Sound and Vibration Toolkit
- LabVIEW

Analysis Capabilities

- Power spectra
- Zoom FFTs
- Fractional-octave analysis
- Vibration-level measurements
- Order spectra
- Transient analysis
- Sound quality

>> For complete specifications, see the *NI USB-443x Specifications* manual at ni.com/manuals.



Overview

The NI USB-4431 is a five-channel dynamic signal acquisition module for making high-accuracy measurements from IEPE sensors. The USB-4431 delivers 100 dB of dynamic range and incorporates software-selectable IEPE (2.1 mA constant current) signal conditioning for accelerometers and microphones. The module consists of four analog input channels for reading from IEPE sensors with a single analog output. The four analog input channels simultaneously acquire at rates from 2 to 102.4 kS/s. In addition, each channel includes built-in antialiasing filters that automatically adjust to your sampling rate. The USB-4431 is ideal for a wide variety of portable test applications such as frequency response audio tests or suspension shaker tests.

Hardware

Each simultaneous signal is buffered, analog prefiltered, and sampled by a 24-bit delta-sigma analog-to-digital converter (ADC) that performs digital filtering with a cutoff frequency that automatically adjusts to your data rate. The USB-4431 features a voltage range of ± 10 V and a dynamic range of 100 dB. In addition, the module can read and write to transducer electronic data sheet (TEDS) Class 1 smart sensors. The USB-4431 has ± 60 V of overvoltage protection and three software-selectable modes of measurement operation: IEPE-on with AC coupling, IEPE-off with AC coupling, and IEPE-off with DC coupling.

The module uses a method of analog-to-digital conversion known as delta-sigma modulation. If, for example, the data rate is 25 kS/s, then

each ADC actually samples its input signal at 3.2 MS/s (128 times the data rate) and produces samples that are applied to a digital filter. This filter then expands the data to 24 bits, rejects signal components greater than 12.5 kHz (the Nyquist frequency), and digitally resamples the data at the chosen data rate of 25 kS/s. This combination of analog and digital filtering provides an accurate representation of desirable signals while rejecting out-of-band signals. The built-in antialiasing filters automatically adjust themselves to discriminate between signals based on the frequency range, or bandwidth, of the signal.

The USB-4431 offers analog output using a delta-sigma modulation digital-to-analog converter (DAC). The overclocking and filtering is done in the digital domain. The now-filtered signal is then output using a DAC. The DAC in the USB-4431 combines high image rejection performance with good flatness in the passband. The analog output also has the flexibility to generate a variety of signals from a DC voltage, to 43.5 kHz sine waves, to arbitrary waveforms.

Analysis Software

The USB-4431 is well-suited for noise and vibration analysis applications. The NI Sound and Vibration Measurement Suite, which specifically addresses these applications, has two components: the NI Sound and Vibration Assistant and LabVIEW analysis VIs (functions) for power spectra, frequency response (FRF), fractional octave analysis, sound-level measurements, order spectra, order maps, order extraction, sensor calibration, human vibration filters, torsional vibration, and sound quality.

Specifications

Analog Input

Input channels	
NI USB-4431	4
NI USB-4432	5
Input connector	1 BNC per channel
ADC resolution	24 bits
ADC type	Delta-sigma
Sampling mode	Simultaneous
Sample rates (f_s)	1 kS/s to 102.4 kS/s in 349.2 μ S/s increments
Sample rate accuracy	± 100 ppm max
Input range	
NI USB-4431	± 10 V _{pk}
NI USB-4432	± 40 V _{pk}
Input protection	± 60 V max

AI Distortion and Noise

Input Signal Frequency (f_m)	THD	THD+N
20 Hz to 20 kHz	-99 dB typ	-90 dB typ
	-93 dB max	-84 dB max
20 Hz to 46.4 kHz	-93 dB typ	-86 dB typ
	-87 dB max	-80 dB max

Analog Output

Output channels	1
AO signal connection	BNC
AO frequency range	DC to 43.5 kHz
AO frequency accuracy	± 100 ppm max
DAC resolution	24 bits
DAC type	Delta-sigma
Output signal range	± 3.5 V _{pk}
Output coupling	DC
Short circuit protection	Indefinite
Minimum working load	1 k Ω
Output impedance	50 Ω

AO Distortion

Update Rate (kS/s)	THD (1 kHz)	THD (20 Hz to 20 kHz)
51.2	-100 dB typ	-89 dB max
80	-97 dB typ	-86 dB max
96	-95 dB typ	-85 dB max

Safety and Compliance

Safety

This product is designed to meet the requirements of the following standards of safety for electrical equipment for measurement, control, and laboratory use:

- IEC 61010-1, EN 61010-1
- UL 61010-1, CSA 61010-1

Note: For UL and other safety certifications, refer to the product label or visit ni.com/certification, search by model number or product line, and click the appropriate link in the Certification column.

Electromagnetic Compatibility

This product meets the requirements of the following EMC standards for electrical equipment for measurement, control, and laboratory use:

- EN 61326 (IEC 61326): Class A emissions; Basic immunity
- EN 55011 (CISPR 11): Group 1, Class A emissions
- AS/NZS CISPR 11: Group 1, Class A emissions
- FCC 47 CFR Part 15B: Class A emissions
- ICES-001: Class A emissions

Note: For EMC compliance, operate this product according to the documentation.

CE Compliance

This product meets the essential requirements of applicable European Directives, as amended for CE marking, as follows:

- 2006/95/EC; Low-Voltage Directive (safety)
- 2004/108/EC; Electromagnetic Compatibility Directive (EMC)

Note: Refer to the Declaration of Conformity (DoC) for this product for any additional regulatory compliance information. To obtain the DoC for this product, visit ni.com/certification, search by model number or product line, and click the appropriate link in the Certification column.

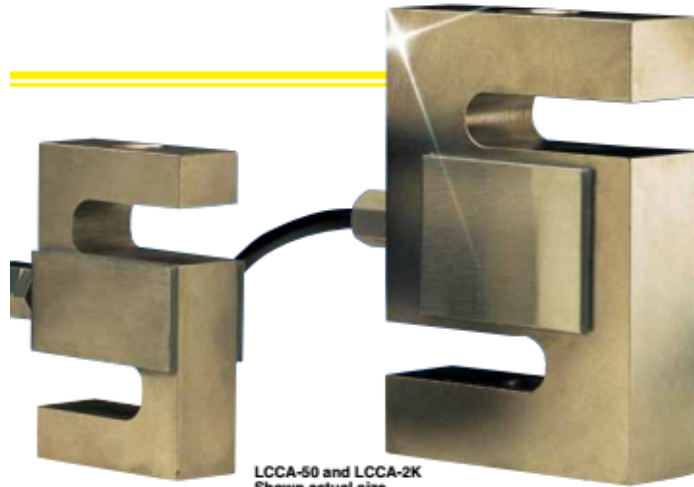
Waste Electrical and Electronic Equipment (WEEE)

EU Customers: At the end of their life cycle, all products must be sent to a WEEE recycling center. For more information about WEEE recycling centers and National Instruments WEEE initiatives, visit ni.com/environment/weee.htm.

Appendix D – Data Sheet of the Load Cell

Page 1 of 1 in the original document. Omega ©. Find document at:

http://www.omega.ca/pptst_eng/LCCA.html



LCCA-50 and LCCA-2K
Shown actual size

Tension/Compression
0-25 to 0-20,000 lb

LCCA Series



- ✓ Environmentally Protected for Washdown Applications
- ✓ Corrosion Resistant
- ✓ Calibration Certificate Supplied
- ✓ 0.25% Interchangeable

SPECIFICATIONS

Rated Output: 3mV/V ±0.0075mV/V
actual output supplied with each load cell)
Excitation: 10 Vdc (15 Vdc maximum)
Accuracy: 0.037% Full Scale
Linearity: 0.03% FS
Hysteresis: 0.02% FS
Repeatability: 0.01% FS
Zero Balance: 1% FS
Creep in 20 min: 0.03% FS
Operating Temperature: 0 to 150°F
Compensated Temperature: 0 to 150°F
Thermal effects: Zero - 0.0015% FS/°F
Span - 0.0008% RDG/°F
Maximum Load: Safe, 150%;
Ultimate, 300%
Bridge Resistance: 350 Ω nominal
Full Scale Deflection: 0.010 in to 0.020 in
Construction: Nickel Plated Carbon Steel
Cable: 20 ft 4-conductor shielded
22-gage wire

(DIMENSIONS IN INCHES)

CAPACITY	A	B	C	D	E
25-200	1/8-28	.65	.50	2.0	2.5
250	1/4-24	.75	.50	2.0	3.0
500-750 1,000-2,000	1/2-20	1.00	.75	2.0	3.0
3,000	3/4-20	1.25	1.00	2.0	3.0
5,000-10,000	1-16	1.25	1.00	3.0	4.25
15,000	1-14	1.50	1.25	4.00	5.50
20,000	1 1/2-12	2.25	2.00	5.00	7.0

WIRING (TENSION) RED: +INPUT
 BLACK: -INPUT
 GREEN: +OUTPUT
 WHITE: -OUTPUT

To Order						
MODEL NO.	RATED CAPACITY	DEFL	WT	COMPATIBLE METERS	LOAD BUTTON MODEL	ROD END MODEL
LCCA-25	25 lb	.015	2 lb	002-S, DP460-S, DP25-S	LBC-014	REC-014M
LCCA-50	50 lb	.015	2 lb	002-S, DP460-S, DP25-S	LBC-014	REC-014M
LCCA-100	100 lb	.010	2 lb	DP3002-S, DP460-S, DP25-S	LBC-014	REC-014M
LCCA-150	150 lb	.010	2 lb	DP3002-S, DP460-S, DP25-S	LBC-014	REC-014M
LCCA-200	200 lb	.010	2 lb	DP3002-S, DP460-S, DP25-S	LBC-014	REC-014M
LCCA-250	250 lb	.010	2 lb	DP41-S, DP3002-S, DP25-S	LBC-038	REC-038M
LCCA-500	500 lb	.010	2 lb	DP41-S, DP3002-S, DP25-S	LBC-012	REC-012M
LCCA-750	750 lb	.010	2 lb	DP41-S, DP3002-S, DP25-S	LBC-012	REC-012M
LCCA-1K	1000 lb	.012	2 lb	DP41-S, DP3002-S, DP25-S	LBC-012	REC-012M
LCCA-2K	2000 lb	.012	3 lb	DP41-S, DP3002-S, DP25-S	LBC-012	REC-012M
LCCA-3K	3000 lb	.012	3 lb	DP41-S, DP87	LBC-012	REC-012M
LCCA-5K	5000 lb	.017	3.5 lb	DP41-S, DP87	LBC-034	REC-034M
LCCA-10K	10000 lb	.017	3.5 lb	DP41-S, DP87	LBC-034	REC-034M
LCCA-15K	15000 lb	.017	6 lb	DP41-S, DP87	LBC-100	REC-100M
LCCA-20K	20000 lb	.017	13 lb	DP41-S, DP87	—	REC-114M

Ordering Example: LCCA-1K is a 1,000 lb capacity load cell.

*Used with DAQ NI USB 6008 and Operational Amplifier Circuit AD620.